FIRST-PRINCIPLES STUDY OF TWO-DIMENSIONAL Mg2C AS AN ANODE MATERIAL FOR METAL-ION BATTERIES

CHU YI ZHI

FACULTY OF SCIENCE
UNIVERSITI MALAYA
KUALA LUMPUR
2022

FIRST-PRINCIPLES STUDY OF TWO-DIMENSIONAL Mg_2C AS AN ANODE MATERIAL FOR METAL-ION BATTERIES

CHU YI ZHI

DISSERTATION SUBMITTED IN FULFILMENT OF THE REQUIREMENTS FOR THE DEGREE OF MASTER OF SCIENCE

DEPARTMENT OF PHYSICS

FACULTY OF SCIENCE

UNIVERSITI MALAYA

KUALA LUMPUR

2022

UNIVERSITI MALAYA
ORIGINAL LITERARY WORK DECLARATION

Name of Candidate: **CHU YI ZHI**

Registration/Matrix No: **SMA190005 / 17202450**

Name of Degree: **MASTER OF SCIENCE**

Title of Dissertation ("this Work"):

FIRST-PRINCIPLES STUDY OF TWO-DIMENSIONAL Mg2C AS AN ANODE MATERIAL FOR METAL-ION

Field of Study:

CONDENSED MATTER PHYSICS (THEORY)

I do solemnly and sincerely declare that:

(1) I am the sole author/writer of this Work;
(2) This work is original;
(3) Any use of any work in which copyright exists was done by way of fair dealing and for permitted purposes and any excerpt or extract from, or reference to or reproduction of any copyright work has been disclosed expressly and sufficiently and the title of the Work and its authorship have been acknowledged in this Work;
(4) I do not have any actual knowledge nor do I ought reasonably to know that the making of this work constitutes an infringement of any copyright work;
(5) I hereby assign all and every rights in the copyright to this Work to the University of Malaya ("UM"), who henceforth shall be owner of the copyright in this Work and that any reproduction or use in any form or by any means whatsoever is prohibited without the written consent of UM having been first had and obtained;
(6) I am fully aware that if in the course of making this Work I have infringed any copyright whether intentionally or otherwise, I may be subject to legal action or any other action as may be determined by UM.

Candidate's Signature Date: 15/2/2022

Subscribed and solemnly declared before,

Witness's Signature Date: 15 Feb 2022

Name:

Designation:

FIRST-PRINCIPLES STUDY OF TWO-DIMENSIONAL Mg_2C AS AN ANODE MATERIAL FOR METAL-ION BATTERIES

ABSTRACT

Owing to their compelling physicochemical and structural properties, two-dimensional (2D) materials have recently emerged as potential candidates for various energy storage and electrochemistry applications. One of the energy storage applications is the anode material for lithium-ion batteries (LIBs). The ever-increasing demand for high-capacity LIBs anode material due to the rapid development of advanced portable electronic devices and electric vehicles have garnered attention on the newly emerged 2D materials as an anode material for LIBs and other metal-ion batteries. Recently, a newly discovered carbide based 2D materials, the 2D Mg_2C has been reported to be exhibiting tunable metallicity. In the present study, first-principles calculations are carried out to investigate the performance of 2D Mg_2C as anode materials for Li, Na, K and Ca-ions batteries. The structure of 2D Mg_2C remained stable upon adsorption of the Li, Na, K, or Ca adatoms as suggested by the calculated binding energies. Encouragingly, the metallic behavior of the adsorbed Mg_2C is desirable to enhance the electric conductivity of 2D Mg_2C as anode materials. The diffusion barriers of the adatoms are calculated to study the diffusivity of the adatoms on the 2D Mg_2C. It is shown that Na and K adatoms exhibits extremely high diffusivity on the 2D Mg_2C with a low energy barrier of 0.08 and 0.04 eV, respectively, which is beneficial for a fast charge/discharge process. The energy barrier for Li and Ca atoms are respectively 0.7 and 0.9 eV, which is about one order of magnitude higher than that of Na and K. Furthermore, for the Na and K atoms, the theoretical

storage capacity can reach up to 1770 $mAhg^{-1}$, two times that of the Li and Ca atom of 885 $mAhg^{-1}$ and nearly five times more than the commercial graphite LIBs (372 $mAhg^{-1}$). It is proposed that the 2D Mg_2C is a promising anode material which offers a fast ion diffusion and high storage capacity.

Keywords: First-principles study, anode materials, 2D materials, batteries

KAJIAN PRISIP PERTAMA TERHADAP Mg_2C BERDUA DIMENSI SEBAGAI BAHAN ANOD BAGI BATERI ION LOGAM

ABSTRAK

Disebabkan sifat fisikokimia dan sifat struktur yang menarik, bahan dua dimensi (2D) telah dianggap sebagai calon yang berpotensi dalam pelbagai aplikasi penyimpanan tenaga dan elektrokimia. Salah satu aplikasi penyimpanan tenaga adalah bahan anod bagi bateri ion lithium (LIBs). Pembangunan yang pantas dalam bidang alat elektronik and kenderaan elektrik telah menyebabkan permintaan LIBs yang berkapasiti tinggi semakin meningkat. Baru-baru ini, bahan 2D berasaskan karbida yang baru ditemui, iaitu 2D Mg_2C telah dilaporkan bersifat logam yang boleh diubahsuaikan. Kajian ini menggunakan prinsip pertama untuk mengkaji kesusuaian dan prestasi 2D Mg_2C sebagai bahan anod bagi bateri ion pelbagai logam. Pengiraan tenaga pengikatan menunjukkan bahawa struktur 2D Mg_2C kekal stabil setelah dijerap oleh adatom Li, Na, K, atau Ca. Tenaga difusi pelbagai atom telah dikira bagi mengkaji sifat difusi atom di permukaan 2D Mg_2C. Kajian ini menunjukkan bahawa atom Na dan K mempunyai tenaga difusi sempadan yang agak rendah iaitu 0.08 dan 0.04 eV masing-masing, di mana ianya merupakan salah satu ciri yang bermanfaat bagi proses caj/discaj yang pantas. Tenaga difusi sempadan bagi atom Li and Ca adalah 0.7 dan 0.9 eV masing-masing. Tambahan pula, kapasiti penyimpanan teori bagi atom Na dan K boleh mencapai setinggi 1770 $mAhg^{-1}$, dua kali lebih daripada atom Li dan Ca yang bernilai 885 $mAhg^{-1}$ dan hampir lima kali lebih daripada grafit komersial (372 $mAhg^{-1}$). Kajian ini mencadangkan bahawa 2D Mg_2C ialah bahan anod berpotensi yang berkapasiti tinggi dan mempunyai difusiviti ion yang tinggi.

Kata Kunci: Falsafah prinsip pertama, bahan anod, bahan 2D, bateri

ACKNOWLEDGEMENT

First and foremost, I would like to express my greatest gratitude to my supervisors, Dr. Chew Khian Hooi and Dr. Yeoh Keat Hoe for the support, guidance and patience throughout the course of this work. The technical guidance by Dr. Yeoh and the academic and scholarly support from Dr. Chew have provided me with a great opportunity to explore computational physics with great fun and pleasure.

I would also like to thank my family for the morale support and encouragement throughout the course of study. Thank you for the constant support and understanding throughout my life. I dedicate this dissertation to my lovely parents and my dear Brownie.

Also, special thanks to Mr. LT Tan. The support, guidance and wise words from you have provided me with so much wisdom and broaden my horizons.

Lastly, my sense of gratitude to one and all, who have directly or indirectly lent their hand in this venture.

TABLE OF CONTENT

ABSTRACT ..... **iii**

ABSTRAK ..... **v**

ACKNOWLEDGEMENT ..... **vi**

LIST OF FIGURES ..... **xi**

LIST OF TABLES ..... **xiii**

LIST OF SYMBOLS AND ABBREVIATION ..... **xiv**

LIST OF APPENDICES ..... **xvi**

CHAPTER 1: INTRODUCTION **1**

1.1 Background of the Research **1**

1.2 Objectives of the Research **3**

1.3 Organization of the Dissertation **4**

CHAPTER 2: LITERATURE REVIEW **6**

2.1 History and Development of LIBs **6**

2.2 Lithiumm-ion Batteries (LIBs) based on 2D Materials **7**

2.2.1 Mono-elemental 2D Materials as Anode Materials of LIBs **8**

2.2.1.1 Graphene **8**

2.2.1.2 Phosphorene, Borophene, Silicene and Stanene 10

2.2.2 Transition Metal Dichalcogenides (TMDs) 11

2.2.3 Transition Metal Carbides, Nitrides or Carbonitrides (MXenes) 12

2.2.4 Emerging New 2D Materials 13

2.3 Na-ion Batteries (NIBs) based on 2D Materials 14

2.4 Potassium-ion Batteries (KIBs) based on 2D Materials 17

2.5 Calcium-ion Batteries (CIBs) based on 2D Materials 19

2.6 The Properties of Emerging 2D Mg_2C 20

2.7 Summary 22

CHAPTER 3: RESEARCH METHODOLOGY 25

3.1 Hohenberg-Kohn Theorems 25

3.2 Kohn-Sham Approach 26

3.3 Kohn-Sham Equation 29

3.3.1 Kinetic Energy Term 29

3.3.2 Hartree Energy Term 30

3.3.3 Exchange-Correlation Energy Term 31

3.4 Exchange-Correlation Functionals 31

3.4.1 Local Density Approximation 31

3.4.2 Generalized Gradient Approximation (GGA) 33

3.5 DFT Limitations 34

3.6 Quantum ESPRESSO Simulation Package 35

3.7 Flow of Quantum ESPRESSO 35

3.8 Convergence Tests 36

3.8.1 Cutoff Energy Convergence Test 36

3.8.2 *k*-points Mesh Convergence Tests 37

3.9 Summary 38

CHAPTER 4: RESULTS AND DISCUSSION 39

4.1 Convergence Tests 39

4.1.1 Cutoff Energy Convergence 40

4.1.2 K-point Convergence 41

4.2 Optimized Structure of 2D Mg_2C 42

4.3 Energy Band Diagrams and Density of States (DOS) 44

4.4 Preferable Adsorption Sites and Binding Energies 46

4.5 Diffusion Profile and Energy Barrier 51

4.6 Binding Energies Between Metal Ions and 2D Mg2C 57

4.7 Theoretical Specific Capacity 59

4.8 Open-Circuit Voltage (OCV) 60

4.9 Comparison of Specific Capacities and Diffusion Barriers ... 62

4.10 Summary 64

CHAPTER 5: CONCLUSIONS AND FUTURE WORK 65

5.1 Conclusion 65

5.2 Future Research 67

5.3 Summary 68

REFERENCES 69

LIST OF PUBLICATIONS AND PAPERS PRESENTED 80

LIST OF FIGURES

Figure 4.1 : Total energy as a function of cutoff energy ……..... 41

Figure 4.2 : Total energy against k-point mesh……. 42

Figure 4.3 : Top view of a 2D Mg_2C supercell, consisting of six high-symmetry sites denote as top C, top Mg, bot Mg, Mg–C bot, Mg–C top and Mg–Mg…… 43

Figure 4.4 : Crystal structure of 2D Mg_2C……... 44

Figure 4.5 : Energy band diagrams and density of states (DOS) of a 2D Mg_2C adsorbed with (a) Li (b) Na (c) K and (d) Ca adatoms…… 45

Figure 4.6 : Top view of a 2D Mg_2C supercell, consisting of six high-symmetry sites denote as Top C, Top Mg, Bot Mg, Mg-C bot, Mg-C top and Mg-Mg…… 48

Figure 4.7 : Diffusion paths for the Li, Na, K and Ca adsorptions on a 2D Mg_2C…….. 53

Figure 4.8 : Diffusion profiles of (a) Li (b) Li (c) K and (d) Ca on 2D Mg_2C…… 54

Figure 4.9 : Atomic structures of the 2D Mg_2CLi, Mg_2CNa, Mg_2CK and Mg_2CCa with different concentrations…….. 56

Figure 4.10 : Binding energy profiles E_B as a function of (a) Li, (b) Na, (c) K and (d) Ca contents in 2D Mg_2C…….. 58

Figure 4.11 : Energy convex hull and voltage profile for (a) Li_xMg_2C (b) Na_xMg_2C (c) K_xMg_2C and (d) Ca_xMg_2C with different stoichiometries……. 62

Figure 4.12 : Comparison on the theoretical maximum capacity of (a) Li (b) Na (c) K and (d) Ca adatoms on a 2D Mg_2C as a function of diffusion barrier for various 2D materials…….. 63

LIST OF TABLES

Table 4.1 : Notation of adsorption site……..... 47

Table 4.2 : Absorption position of metal ions on 2D Mg_2C, binding energy and total energy relative to the Top C site……... 48

Table 4.3: : Specific capacity (C_M), diffusion barrier and OCV for Li, Na, K or Ca on 2D Mg_2C…… 63

LIST OF SYMBOLS AND ABBREVIATION

E_B	:	binding energy
Δ	:	buckling height
E_{cutoff}	:	cutoff energy
E_f	:	formation energy
a,b	:	lattice parameters
C_M	:	theoretical specific capacity
CIBs	:	calcium-ion batteries
CI-NEB	:	climbing-image nudged elastic band
DFT	:	density functional theory
DOS	:	density of states
EV	:	electric vehicle
XC	:	exchange-correlation
GGA	:	generalized gradient approximation
KS	:	Kohn-Sham
LIBs	:	lithium-ion batteries
LDA	:	local density approximation
NEB	:	nudged-elastic band
OCV	:	open-circuit voltage
KIBs	:	potassium-ion batteries
PAW	:	projector-augmented-wave
RGO	:	reduced graphene oxide
NIBs	:	sodium-ion batteries
SEI	:	solid electrolyte interphase
MXenes	:	transition metal carbide, nitrides or carbonitrides

TMDs	:	transition metal dichalcogenides
TEM	:	transmission electron microscope
2D	:	two-dimensional

LIST OF APPENDICES

Appendix A : Input script of Quantum Espresso……..... 81

CHAPTER 1: INTRODUCTION

This chapter presents an introductory research background and the objectives of this research. The intention to investigate the feasibility of the newly predicted material 2D Mg_2C as anode material for metal ions batteries is discussed.

1.1 Background of the Research

Rechargeable lithium-ion batteries (LIBs) are arguably the most important invention in modern technology. They have dominated the portable electronic devices since their first commercial launch by Sony in 1991 (Nishi, 2001). The role of LIBs has become increasing essential especially the growth of electric vehicle (EV) demands the increase in the energy density of the cells such that larger driving distance can be covered. However, current LIBs suffered from limited storage capacity (Jiang et al., 2015) and it would be costly to manufacture large scale battery system employing current LIBs cells owing to the price of lithium salt (Slater et al., 2012). Hence, the search for a higher energy density cell has become a stepping stone to the next generation electronics.

In 2004, Novoselov & Geim exfoliated a few layers of carbon atoms from bulk graphite, known as the graphene and started a revolution in the field of material science. Since then, 2D materials have been playing important role in energy storage application, including supercapacitors, electrochemical storage and metal ion batteries (Mukherjee et al., 2018). Particularly, the idea of employing 2D materials as anode materials for LIBs has been extensively studied since the large surface area could accommodate

more Li ions, thus increasing the energy density of the LIBs cell.

It is shown that 2D materials could achieve higher storage capacity, in addition to other beneficial properties when being used as anode material for LIBs. This includes the structural stability upon the adsorption of the metal ions. For example, phosphorus exhibited a considerably high storage capacity of 1279 $mAhg^{-1}$ (Stan et al., 2013; Sun et al, 2014), but was structural unstable. Phosphorene, a 2D counterpart of bulk phosphorous, on the other hand, demonstrated a capacity of 432.79 $mAhg^{-1}$ while preserving its lattice structure (Li et al., 2015; Yao et al., 2015; Zhao et al., 2014). *In situ* TEM study of LIBs using phosphorene as anode material (Xu et al., 2016) further suggested a method to stabilize the anode material structure using few layers of phosphorene.

Besides searching for better anode materials for LIBs, the search for viable alternative battery system such as sodium ion batteries (NIBs), potassium ion batteries (KIBs), and calcium ion batteries (CIBs) has been widely carried out to reduce the cost of production because these atoms are more abundant than Li metal. In addition, the use of 2D materials as anode material for these metal ion batteries could achieve even better performance than commercial LIBs. This is demonstrated by both the theoretical prediction of NIBs storage capacity of antimonene of about 421.63 $mAhg^{-1}$ (Upadhyay & Srivastava, 2019) and the experimental Na storage capacity of up to 620 $mAhg^{-1}$, which is twice as much the current commercial LIBs storage (Tian et al., 2018).

Besides the most popular group of 2D materials such as the transition metal dichalcogenides (TMDs) and transition metal carbides, nitrides or carbonitrides (MXenes), recently there emerged a new group of carbide-based 2D materials formed with alkaline earth metals. These materials are 2D Be_2C and 2D Mg_2C. Both of these materials exhibited good mechanical strength and electrical properties that is suitable to be considered for anode material application (Li et al., 2014; Naseri et al., 2018; Wang et al., 2018). Furthermore, the theoretical study of 2D Be_2C as an anode material suggested it to be a promising candidate for LIBs anodes (Yeoh et al., 2019). This raised the question whether 2D Mg_2C is also feasible to be the anode material for LIBs and other metal ion batteries.

Thus, in this dissertation, the study of the feasibility of 2D Mg_2C as anode material for LIBs, NIBs, KIBs and CIBs are systematically carried out using first-principles calculations. The study begins with the effects of the adsorption of the Li, Na, K or Ca adatoms on 2D Mg_2C, followed by the study of the storage properties and anode material characteristics.

1.2 Objectives of the Research

Two dimensional (2D) materials have become a research area that gained much attention since its pioneering material, graphene was first successfully isolated from its bulk counterpart, graphite. In this research, first-principles study using density functional theory (DFT) is adopted to design and study the physical and chemical properties of a new carbide-based 2D materials, the 2D Mg_2C. By obtaining the ground state energy of the studied materials through the DFT calculations, the electronic and structural

properties can be subsequently determined.

The objectives of this research are to:

1. Investigate the adsorption of Li, Na, K or Ca adatoms on 2D Mg2C.
2. Study the Li, Na, K or Ca storage properties of 2D Mg_2C.
3. Explore the potential application of the 2D Mg_2C in as battery anodes.

1.3 Organization of the Dissertation

This dissertation reports the research on the feasibility of 2D Mg_2C as an anode material for Li-, Na-, K-, and Ca- ion batteries. There are five chapters in this dissertation. The dissertation begins with the Chapter 1, which shows the brief introduction to the background of the research and the research objectives, followed by the outline of this dissertation.

Chapter 2 gives a literature review on the recent development of anode materials using 2D materials. In this chapter, a comprehensive review from both the theoretical and experimental studies are presented. The mechanical and electrical properties of 2D Mg_2C are also discussed in this chapter.

In Chapter 3, the research methodology employed in this research and several calculations are introduced. The main concept of DFT is discussed in this chapter, including the Kohn-Hohernberg theorem, the derivation of Kohn-Sham equation, and the approximation of the exchange-correlation energies were discussed. The limitation of DFT was also discussed in the last part of this chapter.

Chapter 4 shows the results and discussion of this research. This includes the preliminarily results such as the characteristics of the pristine 2D

Mg_2C, the convergence test, the lattice parameter, energy band structure and density of states. The anode material study is also presented in Chapter 4. This includes the characteristics of 2D Mg_2C upon adsorption, the binding energy, diffusion profile, theoretical specific and open-circuit voltage (OCV). The feasibility of 2D Mg_2C as an anode material for metal ion batteries are presented and discussed.

In the last chapter, the feasibility and suitability of 2D Mg_2C as an anode material for the metal ion batteries is concluded, with recommendations for future projects included in the very last part.

CHAPTER 2: LITERATURE REVIEW

In this chapter, a comprehensive review on the development of 2D material as anode material for metal ion batteries is presented. The literature review starts with the historical background and development of commercial rechargeable LIBs. The following sections discuss the introduction of 2D materials beyond graphene to the LIBs system. A review on the metal ion batteries beyond LIBs employing 2D materials, including the NIBs, KIBs and CIBs are subsequently presented. Next, the discussion on the mechanical and electrical properties of newly predicted 2D materials, and their potential applications as anode materials for metal ion batteries are introduced.

2.1 History and Development of LIBs

Ever since the first presentation of possible storage of electricity by Alessandro Volta in 1800, large efforts have been devoted in the development of the battery. The major challenge in creating an operational and high-efficient battery was the choice of the electrode materials. In the late 70's of the 20^{th} century, several major breakthroughs related to the development of the modern LIBs prototype were achieved. Firstly, the concept of the intercalated cathodes was introduced by Whittingham (1974), also known as the Founding Father of LIBs. He studied the intercalation of the Li ions in transition metal disulphides (1974) and demonstrated a functional rechargeable LIBs using titanium disulphide as anode material (1976). While Whittingham proposed a new generation anode material, using intercalation method, Mizushima, Jones, Wiseman, and Goodenough (1980) discovered

that Li_xCoO_2, another type of intercalated metal chalcogenides to be a promising candidate as cathode material for LIBs. Later on, Yoshino et al. (1985) developed an efficient LIB using petroleum coke as an anode material. Their discoveries on the suitable electrodes for LIBs paved way for the commercial production of LIBs by Sony in 1991 (Nishi, 2001). Nearly about the same time, Fong et al. (1990) showed that using a mixture of propylene carbonate and ethylene carbonate electrolyte, a solid electrolyte interphase (SEI) could form a passivating film on the surface of graphite, protecting it from decomposition during the charge/discharge process. This method allows the commercial rechargeable LIBs with graphite as an anode material achievable, making graphite the next generation anode material for LIBs due to its high energy densities and low maintenance cost (Jiang, et al., 2015).

2.2 Lithiumm-ion Batteries (LIBs) based on 2D Materials

Though graphite is a very popular anode material for rechargeable LIBs owing to its stability, good cycling performance and cost effectiveness, its capacity is limited to 372 $mAhg^{-1}$ due to the limited Li-ion storage sites (Jiang, et al., 2015). To overcome this problem, a new form of material with a thickness of merely a few layers of atoms have garnered great attentions because of their large surface area that could potentially provide more Li-ion storage sites than graphite, thus improving the capacity. These materials are known as 2-Dimensional (2D) materials and the pioneering 2D material, graphene was first successfully exfoliated by Novoselov & Geim in 2004. Besides their large surface area, the unique mechanical and electrical properties of the 2D materials have also distinguished them from their bulk

counterparts and such difference offers material scientists a new category of materials to study. The main characteristics of concerned in this study is the energy storage capacity of 2D materials. Since the successful exfoliation of graphene, more and more 2D materials have been added to this large family, and it can be classified into several groups. Among them, mono-elemental atomic 2D materials, transition metal dichalcogenides (TMDs) and transition metal carbides, nitrides or carbonitrides (MXenes) were the most common groups of 2D materials that could offer wide range of candidates for future electronics. In the following section, the development of different groups of 2D materials as an anode material for LIBs are introduced and discussed.

2.2.1 Mono-elemental 2D Materials as Anode Materials of LIBs

Followed by the successful exfoliation of graphene, there are various mono-elemental atomic 2D materials being subsequently predicted, discovered and theoretically or experimentally studied as anode materials of LIBs. These materials include phosphorene, borophene silicene, and stanene. Experimental study of graphene, phosphorene and their derivatives as anode materials have been readily carried out, while the study of borophene, stanene and silicene remains mostly theoretical.

2.2.1.1 Graphene

The pioneering 2D materials, graphene has been extensively studied for electrochemical applications including the LIBs system. The prediction of graphene-like carbon as anode materials was made by Dahn et al. (1995) a decade prior to the first isolation of graphene. They found that the specific

capacity of single layers of graphene was twice that of graphite (744 $mAhg^{-1}$) due to additional storage site for Li-ion. The method of storing Li-ion in a single layer graphene is also different from graphite. Instead of intercalation of Li-ions, owing to the 2D morphology of graphene, Li-ions are stored in graphene via adsorption mechanism (Winter et al., 1998). Though theoretically exhibiting higher capacity, this method is strongly dependent on the production method of graphene that dictates the number of adsorption sites i.e., the amount of Li-ion stored on graphene-based anodes (Raccichini et al., 2014).

One of the most common methods in producing high-yield and cost-effective graphene in bulk quantities is by the reduction of graphene oxide (Dreyer et al., 2010; Park & Ruoff, 2009; Warner et al, 2013). The reduced graphene oxide (RGO) has also been widely reported as a promising choice for energy storage applications as it demonstrated a high theoretical specific capacity over 2000 $mAhg^{-1}$ (Vargas, 2012). However, the capacity significantly depreciates over few tens of charge/discharge cycle to a capacity even lower than that of graphite (Winter et al., 1998). This is mainly attributed to the formation of solid electrolyte interphase (SEI) as observed in the graphite and other LIBs anode (Winter et al., 1998). Other factors including the restacking of graphene layer that is caused by the reduction in RGO (Vargas, 2012). These drawbacks can be addressed by sorting an effective strategy to produce graphene with higher quality and prevent graphene from re-stacking.

2.2.1.2 Phosphorene, Borophene, Silicene and Stanene

Novel bulk materials have been proven to be able to achieve high specific capacities. However, a large volume expansion could be a drawback which hindered their purpose as anode material. For example, the capacity of black phosphorus can reach up to 1279 $mAhg^{-1}$ (Stan et al., 2013; Sun et al, 2014), but their structural instability has limited the cycling efficiency of battery, thus it is not practical to be selected as anode material. On the other hand, first-principles studies of the lithium adsorption on phosphorene have shown that the lithium atoms could bind strongly to it and demonstrated a capacity of 432.79 $mAhg^{-1}$ without altering its lattice structure (Li et al., 2015; Yao et al., 2015; Zhao et al., 2014). Experimental study of the capability of phosphorene as anode materials was first conducted by Xu et al. (2016) employing *in situ* TEM. Unlike black phosphorus, which pulverized upon Li adsorption, they discovered that the decomposition of the anode material could be overcome by employing several layers of phosphorene, thus, maintain the lattice structure of the anode material.

In addition to graphene and phosphorene, other elemental analogues of graphene such as borophene, silicene and stanene have also been experimentally synthesized (D'vila et al., 2014; Vogt et al., 2012; Zhu et al., 2015). However, due to the synthesis method in producing those materials, which required the deposition on substrates using CVD, the pristine form of those 2D materials do not exist in nature (Shi & Zhao, 2017). In addition, despite the consistency of lattice parameters between the theoretical prediction and experimental data, the intimate interaction between the

substrates and the deposited atomic layer could alter the intrinsic electrical properties of the 2D materials. In this regard, the study of the feasibility of borophene, silicene and stanene as anode materials of LIBs have remained theoretical.

Motivated by the successful synthesis of borophene (Mannix et al., 2015), Jiang et al. (2016) showed that the theoretical capacity of as high as 1860 $mAhg^{-1}$ can be achieved by borophene with an exceptionally low diffusion barrier (2.6 meV). Silicene and stanene resemble the same lattice structure and their predicted theoretical specific capacities for Li ions were 954 and 226 $mAhg^{-1}$ respectively (Mortazavi et al., 2016). The theoretical studies of these elemental 2D materials have shown good specific capacities with low diffusion barrier. In this regard, the search for suitable substrates for the deposition of these 2D materials have been extensively carried out. Zhu et al. (2016) suggested that silicene could be deposited on 2D MgX_2 (X = Cl, Br, I) substrate due to their similar lattice structure. Shi et al. (2016) also proposed graphene as the new substrate for silicene, which could act as a protective layer while providing high mechanical strength, electrical conductivity, and maintaining high capacity and low diffusion barrier.

2.2.2 Transition Metal Dichalcogenides (TMDs)

TMDs are a large group of 2D materials that can be represented by the formula MX_2, where M is a transition metal and X represents a chalcogenic element such as S, Se and Te. To date, there have been more than 40 types of TMDs explored, with MoS_2 being the most studied material

(Shi & Zhao, 2017). The first theoretical investigation of MoS_2 adsorption and diffusion of Li atom was studied by Li et al. (2012). They found that 2D MoS_2 nanosheet exhibited low diffusion barrier for Li atoms indicating higher mobility. Like other 2D materials, when being used as anode materials, 2D MoS_2 could suffer from structural deformation upon lithiation (Shu et al., 2016). Using first-principles calculations, Shu et al. (2016) proposed a graphene/MoS_2/graphene heterostructure to inhibit the deformation of 2D MoS_2 structure upon the intercalation of lithium ions. Experimentally, Xiao et al. (2010) showed that a MoS_2 composite could achieve a capacity up to 100 $mAhg^{-1}$, where a plasma electrolytic oxidation (PEO) layer stabilized the 2D structure. Using the solvothermal method, Hwang et al. (2011) successfully produced MoS_2 nanoplates with graphene-like layers that act as LIBs anodes with a reversible capacity of 700 $mAhg^{-1}$.

2.2.3 Transition Metal Carbides, Nitrides or Carbonitrides (MXenes)

The successful exfoliation of MAX layers has added a new family of 2D material, known as the MXenes to the library of potential anode materials for LIBs owing to their semi-conductive or conductive behavior (Shi & Zhao, 2017). MX in the MAX phase stands for the transition metal carbides/nitrides layer, while A denotes the layer of group IIIA or IVA elements. The general formula of MXenes is $M_{n+1}X_nT_x$-, where M denotes transition metal, X is carbon or nitrogen, T denotes the surface terminating functional groups -F, -OH or -O. The formation of surface termination functional group is the result of the exfoliation method by selective etching from their respective MAX

phase using aqueous HF solution (Lei et al., 2015). Subsequently, the A layers are substituted by those functional groups (-F, -OH or -O), and thus, influencing the intrinsic properties of pristine MXenes.

The first theoretical study of lithium storage in pristine Ti_3C_2 and its composite was carried out by Tang et al. (2012). They showed that the pristine Ti_3C_2 demonstrated a theoretical specific capacity of 320 $mAhg^{-1}$ and diffusion barrier of 70 meV. The presence of termination surface functional group was found to decrease the storage capacity and also hindered the diffusion of lithium ions (Tang et al., 2012). Later, using DFT, Er et al. (2014) demonstrated the capability of Ti_3C_2 as anode materials for metal ion batteries and showed that a capacity of 447.8, 351.8, 191.8, and 319.8 $mAhg^{-1}$ respectively for LIBs, NIBs, KIBs and CIBs could be achieved by Ti_3C_2 MXenes. Experimental studies have been carried out to determine and improve the performance of Ti_3C_2 as LIBs anode material. Experimentally, Sun et al. (2014) reported the capacity of 123.6 $mAhg^{-1}$, while Xie et al. (2014) suggested the Ti_3C_2 terminated with -O groups could achieve a larger Li ion storage capacity. In brief, the functional group captioned to the MXenes could significantly affect the performance of an anode material.

2.2.4 Emerging New 2D Materials

The experimental implementation of graphene, phosphorene, MoS_2 and Ti_3C_2 has boosted the research on other novel 2D materials as anode materials for LIBs. Currently, the anode material study of these materials remain mostly theoretical based. Monolayer MoN_2 and GaN were predicted

to produce LIBs with theoretical capacity of 432, and 938 $mAhg^{-1}$ respectively with the Li diffusion barriers in the range of 0.068 to 0.78 eV (Zhang, et al., 2016; Zhang et al., 2018). Recently, h-BAs was also considered a potential candidate for LIBs anode material with a capacity of 522 $mAhg^{-1}$ and diffusion barrier of 522 meV (Khossossi et al., 2019). Zhang et al. (2020) demonstrated the capability of single layer PC_6 as anode materials using first-principles method, showing a theoretical specific capacity of 717.09 $mAhg^{-1}$. The potential application of WSe_2 as LIBs anode material was studied by Rehman et al. (2019) The predicted capacity and Li diffusion barrier were 144 and 240 meV, respectively. Karmakar et al. (2016) revealed that 2D SiSe have a low Li diffusion barrier of ~0.15 eV while having specific capacity of 250.44 $mAhg^{-1}$. The reported 2D materials here demonstrated satisfactory anode material characteristics that are comparable or even better than graphite in terms of theoretical specific capacity and diffusion barrier.

2.3 Na-ion Batteries (NIBs) based on 2D Materials

While LIBs are dominating the portable energy storage industry, there are several deficiencies posed by the LIB systems that have become major concerns. This includes the scarcity of Li reserve that leads to the relatively high cost of lithium salt, the high reactivity of Li atoms and flammability of organic electrolytes, and the method of disposal of spent cell that caused environmental hazard (Scrosati et al., 2011; Slater et al., 2012). The development of sodium ion batteries (NIBs) has become a cheaper alternative to conventional LIBs, because compared to Li, Na is highly

abundance and cost effective, making it a promising candidate for large-scale electrical energy storage systems (Slater et al., 2012). However, due to its larger ionic radius as compared to that of Li, Na ions are unable to intercalate into the graphite layer. Besides, the larger ionic radius also could result in sluggish diffusivity and large area expansion during the sodiation/desodiation process in other anode materials. Thus, it requires a suitable anode material other than graphite.

The discovery of 2D materials could offer a variety of choices to the NIBs anode material. RGO, as anode material of NIBs, was reported to have good life cycle, promising electrochemical behavior and exceptional rate capability (Wang et al., 2013). Ding et al. (2013) also reported the synthesis of various kind of few-layer graphene and showed that these graphene-like materials exhibited specific capacity of about 300 $mAhg^{-1}$. Their study has demonstrated the possibility of 2D material as an anode material for NIBs.

Besides graphene, other mono-elemental 2D materials are expected to demonstrate exceptional properties as anode materials for NIBs. Upadhyay & Srivastava (2019) investigated antimonene for anode application in SIBs and found that the semiconducting nature of antimonene was shifted to metallic upon sodiation, which is favorable for energy storage application. They reported the maximum theoretical specific capacity of 421.63 $mAhg^{-1}$ and diffusion barrier of 0.12 eV. Encouragingly, the experimental study of 2D antimonene has demonstrated a Na storage capacity up to 620 $mAhg^{-1}$ (Tian et al., 2018), which is higher than the theoretical predicted value.

MoS_2 is among the most widely studied TMDs in battery application, including NIBs. The intercalation of Na ions into 2D MoS_2 was studied by Mortazavi et al. (2014) and Li et al. (2017) using the first-principles methods. Later on, experimental anode material study using MoS_2 was conducted by several groups. Su et al. (2015) and Bang et al. (2014) respectively reported a reversible specific capacity of 386 $mAhg^{-1}$ and 254 $mAhg^{-1}$ using different exfoliation methods.

Other novel 2D materials were also reported to be a feasible choice as the anode material of NIBs. For instance, 2D GeP_3 exhibits an exceptional high specific capacity of 1295.43 $mAhg^{-1}$, while suffers from a relatively high diffusion barrier (Deng et al., 2019). Wang et al. (2018) predicted the theoretical specific capacity of 2D VO_2 to be 613 $mAhg^{-1}$ with a diffusion barrier of 98 meV. Besides that, monolayer Mn_2C was reported to have a low diffusion barrier of 22 meV with the Na ion storage capacity of 443.6 $mAhg^{-1}$ (Zhang et al., 2020). Theoretical studies by Liu et al. (2018) revealed that borophene exhibits an exceptionally high Na-ion capacity of 1240 $mAhg^{-1}$ upon achieving full sodiation. The capacity of NIBs using arsenene and monolayer β-GeSe anode were predicted to be 1073.18 and 353.65 $mAhg^{-1}$ respectively (Benzidi et al., 2019; Zhou et al., 2018). Besides that, Ti_3C_2 also possessed a capacity of 351.8 $mAhg^{-1}$ with a diffusion barrier of 96 meV (Er et al.,2014).

2.4 Potassium-ion Batteries (KIBs) based on 2D Materials

It is interesting to note that KIBs naturally has long been a crucial system in the living mechanisms of plants, where K ions serve as the primary charge carrier in the plants and the energy storage in the plants relies on the circulation of K ions (Gajdanowicz et al., 2010). In addition to NIBs, KIBs have also been proposed as the next generation battery, mainly attributed to two reasons. Firstly, the abundance of potassium (Wu et al., 2017) and the usage of aluminum foil as current collector instead of copper foil in LIBs (Vaalma, et al., 2018) have made the cost of producing KIBs much cheaper than LIBs. Secondly, Kubota et al. (2018) demonstrated the ionic mobility and conductivity of K ions to be the highest among Li and Na-ions. Thus, replacing Li ions with K ions would allow us to enhance the performance of battery systems in terms of rate capability.

In contrast to the commercial LIBs, however, the storage capacity of KIBs was relatively low at 250 $mAhg^{-1}$ due to the larger ionic radius (Jian et al., 2015). Using nitrogen-doped graphene, Share et al. (2016) successfully enhanced the K ion storage capacity from 278 to 350 $mAhg^{-1}$. Besides that, experimentally, Ji et al. (2020) have demonstrated the full cell prototype for $KFeC_2O_4$ cathode to deliver a reversible capacity of about 85 $mAhg^{-1}$ with long cyclability and good stability.

Zhang et al. (2019) summarized the main challenges that hindered the application of KIBs. It is found that volume expansion of graphite anode of above 60% was observed (Jian et al., 2015). The large expansion of volume could lead to the formation of SEI that consumed the electrolyte. The solvent in the KIBs electrolyte could be reduced on the electrode surface

due to the low electrochemical potential of K ions (Komaba et al., 2015). This is known as the side reactions. The sluggish kinetics reaction of K ions due to the large ionic radius also resulted in the decline of rate capability, further causing the formation of SEI which eventually fading the capacity.

Recently, 2D materials have been proven to alleviate the volume expansion problems and enhance the reaction kinetics for sulfur/selenium-based electrodes to some extent (Zhang et al., 2019). By decreasing the thickness of Sb_2S_3 nanosheets, Zhang et al. (2019) were able to shorten the K ions diffusion pathway, thus, increasing the rate capability of KIBs. This encourages the introduction of 2D materials to KIBs. In this regard, theoretical studies of MXenes and TMDs as anode material for KIBs were reported. Using first-principles calculations, Er et al. (2014) investigated the Ti_3C_2 MXene and demonstrated a theoretical capacity of 191.8 $mAhg^{-1}$ for KIBs with a diffusion barrier of 0.103 eV. Wang et al. (2017) also showed that 2D VS_2, one of the TMDs, exhibited a capacity of 466 $mAhg^{-1}$ with diffusion barrier of 0.061 eV.

Besides that, other novel 2D materials also demonstrated feasible characteristics for KIBs anode material. For instance, the KIBs storage capacity of 2D FeSe was reported to be 315 $mAhg^{-1}$ and the diffusion barrier was 0.11 eV (Lv et al., 2020). Wang et al. showed that 2D Si_3C exhibited an exceptionally high specific capacity of 836 $mAhg^{-1}$ for KIBs with a diffusion barrier of 0.11 eV (Wang & Li, 2020). Zhou et al. (2018) predicted the capacity of KIBs using monolayer β-GeSe anode was to be 353.65 $mAhg^{-1}$ while Li et al. (2016) showed that germanium sulfide nanosheet

exhibited a theoretical capacity of 256 $mAhg^{-1}$ and a diffusion barrier of 0.005 eV (Li et al., 2016). Boron phosphide monolayer was also predicted to have a capacity up to 570 $mAhg^{-1}$ with a diffusion barrier of 0.155 eV (Jiang et al., 2017).

2.5 Calcium-ion Batteries (CIBs) based on 2D Materials

Multivalent ions such as divalent ions (Mg^{2+}, Ca^{2+}) and trivalent ions (Al^{3+}) have been suggested as the alternatives to Li ions in energy storage system because of the possibility of demonstrating a higher storage capacity due to the multivalency of charges (Gummow et al., 2018). Recent studies on multivalent ion batteries have been focused on Mg ions since their ionic radius is similar to that of Li ions, such that the anode materials used by current LIBs could be potentially intercalated by them. However, it suffers from low energy density and extensive research has to be carried out before they can be commercially viable. On the other hand, with the lack of suitable electrolytes for Al ion battery, the experimental research on Al ion batteries is still at its early stage (Gummow et al., 2018).

While being more abundant than Li, Na and K, Ca is a readily available material that could significantly reduce the cost of bulk battery production. In addition, owing to the nontoxic nature of Ca, the manufacturing of CIBs would not pose environmental hazard (Gummow et al., 2018).

The intercalation of Ca into graphite, the most common anode material for LIBs, was studied by Park et al. (2019). They showed that the

full intercalation of Ca could deliver a capacity up to 87 $mAhg^{-1}$ without significant degradation over a long cycle. However, this value is much lower than that of commercial LIBs. Ponrouch et al. (2016) reported Ca ion could exhibit a storage capacity of 400 $mAhg^{-1}$, which could be achieved using Ca-alloying Si ($CaSi_2$). These experimental reported capacities of novel materials are lower than that of commercial LIBs.

The theoretical prediction of Ti_3C_2 as anode materials for CIBs that conducted by Er et al. (2014) reported the theoretical specific capacity and diffusion barrier to be 319.8 $mAhg^{-1}$ and 0.118 eV, respectively. Mortazavi et al. (2016) showed that borophene exhibited a theoretical specific capacity of 800 $mAhg^{-1}$ as CIBs. Besides that, Vakili-Nezhaad et al. (2019) showed that the theoretical specific capacity of 2D WS_2 to be 326 $mAhg^{-1}$. Using DFT calculations, Rao et al. (2019) demonstrated an exceptionally high specific capacity of 1256 $mAhg^{-1}$ with a low diffusion barrier of 0.22 eV. The theoretical studies showed that 2D materials as CIBs anode could achieve comparable or higher storage capacity than the commercial LIBs.

2.6 The Properties of Emerging 2D Mg_2C

The study of the bulk Mg-C material has been carried out systematically and thoroughly in the past. In the bulk system, magnesium carbide can exist in at least four different configurations with different chemical and optical properties, namely the acetylide-type MgC, monoclinic β-Mg2C3 (space group C2/m), orthorhombic α-Mg2C3 (space group Pnnm) and antifluorite Mg_2C (Meng et al., 2017).

However, the research on the 2D system of magnesium carbide is very limited compared to its bulk counterpart until the first theoretical investigation on the electronic properties of 2D magnesium carbide, (Mg_2C) using DFT was conducted by Naseri (2017). He predicted the structural stability of 2D Mg_2C, adding it to the new family member of group-IIA-IVA 2D system. This newly predicted material resembles the structure of another material that was previously discovered, known as the 2D Be_2C (Li et al., 2014; Naseri et al., 2018). Belonging to the same group in the periodic table, both 2D Be_2C and Mg_2C 2D Mg_2C are quasi-planar hexacoordinate moiety alkaline-earth carbide-based 2D material consisting a C atom that binds to six Be or Mg atoms. Meng et al. (2017) later carried out a comprehensive and systematic study on its physical and optical properties and provided a detailed insight into this newly discovered structure. They revealed that 2D Mg_2C has an excellent mechanical stability with negative Poisson's ratio under the influence of tensile strain in the zigzag direction (Wang et al., 2018). The phonon dispersion also indicates the absence of the negative frequency implying the structural stability of the 2D Mg_2C. In addition, they have also carried out ab initio MD simulations and found that the crystal structure of 2D Mg_2C is preserved up to 900 K.

Interestingly, not only this material exhibits mechanical stability, they also discovered that under different degree of biaxial strain, 2D Mg_2C can even host up to three different phases, (i.e., semiconducting, semi-metallic, and metallic phase), which further encouraging the experimental synthesis of 2D Mg_2C for future nanotechnology applications, especially for the

energy storage application. The metallic phase could be beneficial for ionic diffusion in the battery charging/discharge process.

Encouragingly, using first-principles calculations, Yeoh et al. (2019) showed that 2D Be_2C, the counterpart of 2D Mg_2C with Be atom substitute, is feasible to be employed as an anode material for LIBs, with a theoretical specific capacity as high as 1785 $mAhg^{-1}$ and a low diffusion barrier of 0.11 eV. The exceptional features of 2D Mg_2C, alongside with the feasibility of 2D Be_2C as LIBs anode and the recent development of metal ion batteries beyond graphene have motivated the present study to examine the potential application of 2D Mg_2C as LIBs, as well as other metal ion anode materials.

2.7 Summary

In brief, the discoveries of rechargeable LIBs in the 1970's with high energy densities and low maintenance cost has revolutionized the energy storage application. The capacity of graphite anode is limited which inspired the search for better anode material to meet the ever-increasing demand of highly efficient energy storage devices.

Due to the large surface area of 2D materials, which could have more active storage site to accommodate more Li ions, they have become potential candidates for next generation LIBs. The performance (stability, theoretical specific capacity, diffusion barrier) of some other mono-elemental 2D materials, MXenes, TMDs and other novel 2D materials as LIBs anode materials are also presented. Interestingly, theoretical and experimental studies of 2D materials as LIBs anode have shown promising

outcomes which encourages further experimental study to improve the production method of 2D materials to be utilized as anode material.

This chapter also presented the recent development of metal ion batteries beyond LIBs. The relatively high cost of Li salt can be ascribed to its scarcity that requires the alternatives that are relatively cheaper for vast production of battery system. NIBs, KIBs and CIBs are alternatives to LIBs owing to the abundance of the metal ions in earth's crusts if compared to Li ion. In addition, multivalent ions could also be beneficial for battery application in providing higher capacity. However, limitations of metal ion batteries include the volume expansion of electrodes and lower capacity. 2D materials are proven to address the problem to some extent. Experimentally studies of metal ions batteries using 2D materials as anode showed that they could deliver capacities comparable or higher than that of commercial LIBs. The theoretical specific capacities, diffusion barriers of the 2D anode materials for metal ion batteries beyond LIBs were reported.

It is noted that the most common problems faced by 2D and other novel anode materials are the formation of SEI on the surface of electrodes. This passivating film is a double-edged sword, because it stabilized the structure of anode material, but on the other hand, could consume the electrodes, thus hindering the application as anode material.

The mechanical and electrical properties of the newly discovered 2D Mg_2C was discussed in the last section of this chapter. The strong mechanical stability as demonstrated by the negative Poisson's ratio, and its tunable metallicity shows good potential to be studied as metal ions

battery anode material. Also, the reported properties of 2D Be_2C as LIBs anode materials motivates the present study of 2D Mg_2C as anode materials.

CHAPTER 3: RESEARCH METHODOLOGY

This chapter outlines the computational methods employed in this project. A brief introduction to the DFT was discussed, followed by the introduction to the Quantum ESPRESSO simulation package. Several calculations and the key parameters, including the vacuum slab insertion, diffusion path determination, and energy band diagram are discussed in this chapter.

3.1 Hohenberg-Kohn Theorems

The solution to many-electron system from Schrödinger's equation was complicated due to the complexity when solving the Schrödinger's equation for a many-body system. In 1964, Hohernberg and Kohn proposed two simple theorems that laid the foundation of DFT (Hohenberg & Kohn, 1964). These two theorems are:

1. A unique external potential can be determined based on the ground state electron density.
2. An exact ground state energy can be determined when the system energy is minimized with respect to the electron density.

They have proven that the external potential is a unique functional of ground state electron density, which established a one-to-one matching between electron densities and the external potentials. The second theorem offered an approach to obtain the ground state energy of a system using variational principle with respect to the electron density. Thus, by the means of obtaining the ground state electron density one can determine the external potential of the system and the ground state energy, and hence other properties of a system by solving Schrödinger's equation.

3.2 Kohn-Sham Approach

While Hohenberg and Kohn proposed the unique relation between ground state electron and external potential, Kohn and Sham took one step by spending another year to develop approximation methods for treating an inhomogeneous system of interacting electrons, which led to self-consistent equations (Kohn & Sham, 1965). They established a fictitious one-electron system in contrast to the real many-electron system. By doing so they reconstructed the Hamiltonian and Schrödinger's equation. In this and the following section, we will discuss the method Kohn and Sham addressing the many-electron system and the resulting Kohn-Sham equation.

Consider the Hamiltonian of an *n*-electron system, in atomic unit:

$$\widehat{H} = -\frac{1}{2}\sum_{i=1}^{n}\nabla_i^2 - \sum_{I=1}^{N}\sum_{i=1}^{n}\frac{Z_I}{|\vec{r_i} - \vec{r_I}|} + \frac{1}{2}\sum_{i\neq j}^{n}\frac{1}{|\vec{r_i} - \vec{r_j}|} \qquad (3.1)$$

The first term on the right-hand side of Equation (3.1) is the kinetic energy of the electrons and nuclei. Since the mass of nuclei is significantly heavier than that of electrons, the motion of nuclei is much slower than the motion of electrons. Thus, the nuclei are assumed to be stationary. This is known as the Born-Oppenheimer approximation. The reason to this is to speed up the computation of wavefunctions involving large number of atoms, else it would be computational expensive to study a quantum mechanical system. Thus, the first term is the summation of the kinetic energy of all the electrons. The second term deals with the electron-nuclei Coulombic interaction, which is regarded as the external potential. The last term describes the interaction between an electron and the mean electric potential generated by other electrons using mean-field approximation, i.e., the Hatree potential.

The summation of the last term covers the electrons for $i \neq j$ such that any self-interaction is excluded while factor "1/2" in the last term arises accounts for the correction for the double counting.

Using the Hatree-Fock approach (Hatree, 1928), we can estimate the interacting *n*-electron energy by considering the energy term as follow:

$$E = T + E_{ext} + E_H + E_X \tag{3.2}$$

where T, E_{ext}, E_H and E_x are respectively the kinetic energy, external energy, Hatree energy and the exchange energy term.

To avoid the coupled interaction between all *n* electrons, Kohn and Sham assumed that all electrons are at their ground state and non-interacting. In reality, the electrons are interacting with each other. The interaction is accounted for by treating the electrons interacting with an effective potential. It is the method of mapping the *n*-electron (interacting) to the one-electron (non-interacting) system under the appropriate external potential. The energy terms can be further evaluated as:

$$T = T^{non} + T^{int} \tag{3.3}$$

and

$$E_H + E_X \rightarrow E_H + E_X + E_c^{int} \tag{3.4}$$

where T^{non},T^{int} ,E^{int} are respectively the non-interacting kinetic energy, interacting kinetic energy and interacting correlation energy.

Combining the coupled terms as a single term, we have the exchange-correlation energy:

$$E_{XC} = E_X + E_c^{int} + T^{int} = E_X + E_C \tag{3.5}$$

The correlation energy, E_c is the constituent of interacting correlation and kinetic energy, both are energies due to the correlation. It represents the correlation effect arises from the kinetic and electron-electron interaction.

Combining Equations (3.3), (3.4) and (3.5), the total energy of the interacting *n*-electron system can be expressed as:

$$E = T^{non} + E_H + E_{XC} + E_{ext} = E = G[\rho(\vec{r})] + E_{ext} \tag{3.6}$$

where the first three terms on the right-hand side of the equation can be calculated by combining them to be expressed as $G[\rho(\vec{r})]$, which is a universal functional of electron density. This functional can be calculated by using variational principle with respect to electron density, shall be discussed in the next section. The complication in calculating the total energy of the *n*-interacting electron system arises from the last term, the external energy, E_{ext}, as it is an unknown term subject to approximation. The total energy in Equation (3.6) can be further modified by including the Coulombic repulsive energy between the nuclei by adding a constant, subject to the Born-Oppenheimer approximation.

The whole idea of Kohn-Sham approach in solving the *n*-electron system is as follows:

1. Set an initial guess of electron density $\rho(\vec{r})$.
2. Constructing the Kohn-Sham Hamiltonian using Equation (3.6) with an unknown E_{ext}

3. Solve for the eigenvalue for the Kohn-Sham equation.
4. Inspect the convergence of the newly generated electron density $\rho_2(\vec{r})$. If $\rho_2(\vec{r})$ is converged, we have solved for the total energy of the system.

3.3 Kohn-Sham Equation

In previous section, we have defined each of the energy terms to be the functional of electron density. Thus, in this section, we will derive Kohn-Sham equation by defining the energy functional in Equation (3.6) and takes its derivatives with respect to electron density, using variational principle.

3.3.1 Kinetic Energy Term

Following the Kohn-Sham (KS) approach, they derived a new set single particle Schrödinger's equation by reintroducing the wavefunction as the KS orbital, φ_i with:

$$\rho(\vec{r}) = \sum_{i=1}^{n} \langle \varphi_i | \varphi_i \rangle \tag{3.7}$$

where *n* is the number of number of electrons and $\rho(\vec{r})$ is the electron density computed by taking the probability density of the orbital φ_i. Thus, the kinetic energy, T is given by:

$$T[\rho(\vec{r})] = -\frac{1}{2}\sum_{i=1}^{n} \langle \varphi_i | \nabla^2 | \varphi_i \rangle \tag{3.8}$$

Since the electron density $\rho(\vec{r})$ is a function of orbital wavefunction, we can now see that the kinetic energy is in fact a functional of $\rho(\vec{r})$.

3.3.2 Hartree Energy Term

In a non-interacting electron distribution, the Hartree potential arises from the interaction between an electron at position $\vec{r}$ and the mean electron density at position $\overrightarrow{r'}$ under mean field approximation.

$$U_H(\vec{r}) = \int \frac{\rho(\overrightarrow{r'})}{|\vec{r}-\overrightarrow{r'}|} d\vec{r} \tag{3.9}$$

We can now express the expectation value of Hartree energy with reference to the Hartree potential derived in Equation (3.9).

$$E_H[\rho(\vec{r})] = \langle \varphi_i | U_H | \varphi_i \rangle = \frac{1}{2} \iint \frac{\rho(\vec{r})\rho(\overrightarrow{r'})}{\left|\vec{r} - \overrightarrow{r'}\right|} d \tag{3.10}$$

Using the Poisson's equation, we can express the Hartree potential in terms of electron density:

$$\nabla^2 U_H(\vec{r}) = -4\pi\rho(\vec{r}) \tag{3.11}$$

The mean-field in Equation (3.11) is generated by all other electrons, results in the expectation value for Hartree energy to be classical and Coulombic. In this equation, the unrealistic and unphysical self-interaction of electron is taken into account since the generated mean-field considers the effect of all individual electron, i.e., the electron is "interacting" in the mean-field contributed by itself. This self-interaction problem could be resolved in the following section by considering the exchange energy term.

3.3.3 Exchange-Correlation Energy Term

The exchange-correlation energy takes into account of all quantum effects. Recall Equation (3.5), it is the energy term of exchange energy and interacting kinetic and correlation energy. The exchange energy, E_x is the exchange energy between electrons with the same spin, which is associated with the Pauli exclusion principle, while correlation energy, *Ec* deals with the correlation energy of electrons with different spin. The corresponding wavefunction has the nature of antisymmetric. Thus, the exchange energy is given by:

$$E_X = -\frac{1}{2}\sum_{i}^{n}\sum_{j}^{n}\iint \frac{\varphi_i^*(\vec{r})\varphi_i^*(\vec{r'})\varphi_i(\overrightarrow{r'})\varphi_j(\vec{r})}{\left|\vec{r}-\overrightarrow{r'}\right|}d\vec{r}d\overrightarrow{r'} \qquad (3.12)$$

Equation (3.12) , E_X is the function of the single-particle orbitals taken as the summation of four-center integrals. The result of this equation is that the overlapping of electron densities near the reference electron is lessened, causing the repulsion energy between electrons decreased, eventually which eventually leads to the attractive force.

3.4 Exchange-Correlation Functionals

3.4.1 Local Density Approximation

To solve for the electron density of a many-body system, the simplest way to approximate the electron density is to assume it to be constant and not varying at a localized scale, known as the Local Density Approximation (LDA). The idea is that the many-electron system can be divided into many regions of uniform electron density with different density value. This means that for an electron in a particular localized region it experiences the same

overall effect exerted by other electrons in that particular piece. Hence, the total XC energy can be subsequently determined by taking the summation of the energy terms associated with these discrete local elements. A more realistic approach, known as the generalized gradient approximation, will be discussed in the further section.

$$E_{XC}^{LDA}[\rho(\vec{r})] = \int \rho(\vec{r})\, \varepsilon_{XC}^{hom}[\rho(\vec{r})] d\vec{r} \tag{3.13}$$

Equation (3.13) shows the general formula for the approximation of XC energy using LDA. For a system with small variation in electron density such as simple metals and covalent systems, LDA give a surprisingly accurate calculations which consistent with experimental results, despite it being a very simple approximation. The reason is that for LDA it tends to overestimate the E_X while underestimates E_C. Recall Equation (3.5), since the XC energy is the summation of both E_X and E_C, the overall effect of over/under estimation is neutralized, giving a good estimation of the whole XC energy.

However, LDA suffers from several drawbacks owing to the overestimation or underestimation of individual energy terms (E_X and E_C). This includes the underestimation of several parameters such as the lattice parameters, and the energy bandgap of a semiconducting system. In addition, for strongly correlated systems, transition metals, van der Waals materials and materials with weak hydrogen bond, LDA has failed to address the total energy of such systems, where the effect of variation in electron density is strong and cannot be neglected.

3.4.2 Generalized Gradient Approximation (GGA)

In previous section we have discussed the simple approximation that assumes the electron density to be locally uniform. In the real systems, however, the electron density is inhomogeneous with varying density across the whole system. Thus, a more accurate approximation known as the Generalized Gradient Approximation (GGA) is adopted to generate a XC functional with higher accuracy. Unlike LDA which provides only localized density information, GGA describes both the local and semi local information of electron density by taking account both the local electron density and the density gradient at a particular location. The inclusion of density gradient should in principle provide a better outline of the many-electron system, hence generating a more accurate result. The GGA formula is similar to Equation (3.13), except with an additional variable:

$$E_{XC}^{GGA}[\rho(\vec{r})] = \int \rho(\vec{r})\, \varepsilon_{XC}^{GGA}\left[\rho(\vec{r}), \rho\left(\overrightarrow{r'}\right)\right] d\vec{r} \tag{3.14}$$

GGA works well with almost every system in providing most structural properties with an error within 1~3%. In addition, the lattice parameters generated using GGA are more accurate without facing the overbinding problem as in the case of LDA. In spite the accuracy in predicting the structural properties of almost all system, GGA suffers a main drawback which is the underestimation of energy bandgap. This can be overcome by performing bandgap correction calculation.

In summary, there are numerous assumptions made in the derivation of Kohn-Sham equation. First, the derivation of the Kohn-Sham equation is based on the construction of a fictitious one-electron system where the

electrons are non-interacting. This allows us to avoid solving a many-body problem, which is otherwise a complicated process. Secondly, the Born-Oppenheimer approximation treats the nuclei to be stationary to further simplify the Hamiltonian to be solved. In addition, the exchange-correlation functional is introduced to reflect the electrons' interaction. LDA assumes that the electrons are localized, such that the electron density does not vary with respect to position. This assumption provides a simple yet elegant picture of the system of simple metals and covalent systems. In addition, a more realistic XC functional known as GGA takes the variation of electron density into consideration, thus, providing more accurate results than that of LDA.

3.5 DFT Limitations

In the formulation of the Kohn-Sham equation under the DFT framework, there involves several assumptions and approximations (the Born-Oppenheimer approximation, the XC energy term approximation, the non-relativistic approximation). In addition, the implementation of the XC functional relies on the approximation of electron density (LDA and GGA). Thus, choosing an appropriate pseudopotential based on the XC functional is crucial in order to obtain a more reliable system. The choice of the pseudopotential, which is the main source of the error due to the exact XC energy being unknown, but rather an approximation, depends heavily on the system, in order to produce a more accurate result. With different XC functionals employed in the calculation one might expect deviation in the computational results, such as the total energy and the band structure of the system. Hence, this requires careful consideration and justification from

many aspects such as the phase of the system of interest, the accuracy of the computational results, the computational cost and etc. Nevertheless, DFT is proved to be a powerful tool in material science, especially in computational chemistry and physics when dealing with many-electron quantum system in predicting the electronic, mechanical and optical properties of a system, with careful study and adoption of appropriate XC functionals.

3.6 Quantum ESPRESSO Simulation Package

In this research, all DFT calculations were performed using Quantum ESPRESSO (Quantum open-source package for research in electronic structure, simulation, and optimization) software packages (Giannozzi, 2017) (Giannozzi et al., 2009). It is a distribution (an integrated suite) of software for first-principle DFT simulations, i.e., atomistic calculations based on electronic structure, using a plane-wave basis set and pseudopotentials. We use PWscf (plane-wave self-consistent field) packages to perform total energy calculations and nudged-elastic band (NEB) calculations, which shall be further discussed in the following sections. It has been proven to provide accurate simulation for theoretical and computational material research.

3.7 Flow of Quantum ESPRESSO

The following shows the flow of a calculation run by using Quantum ESPRESSO:

1. Choose an appropriate pseudopotential and XC functional to construct an initial predicted electron density.
2. The expansion of KS orbitals using a plane wave (PW) basis set to calculate the T^{non} and the external potential at the given atomic position

in a crystal structure.

3. Calculate the Hartree potential and the XC potential to construct the KS Hamiltonian.
4. Solve for the KS equations using iteration method in the real and reciprocal spaces.
5. Using the newly generated orbitals, calculate the new electron density. If self-consistency is achieved, we have calculated the ground state energy of the system with the ground state electron density.

3.8 Convergence Tests

The main objective of a DFT calculation is to obtain the system's ground state energy with respect to the electron density, i.e., the energy gradually decreases to a final value that subjected to the perturbation of electron density. Thus, one has to ensure the energy is converging to a certain minimal value throughout the iteration. It is therefore crucial to perform a proper convergence test to prevent the divergence of energy value before the study of system can be carried out. There are two convergence tests to be carried out, the cutoff energy and k-points mesh convergence test.

3.8.1 Cutoff Energy Convergence Test

Quantum ESPRESSO uses plane-wave basis to construct the pseudopotential of an element. A perfect pseudopotential, in principle, can be constructed with a full set of plane waves. However, a full set plane wave basis can be expressed with an infinite number of plane waves. This is impractical in DFT calculation owing to high computational cost and time consuming. Thus, instead of taking into account of all plane-waves, one can

choose to consider only certain sets of plane waves that fulfills the cutoff criteria:

$$E_{cutoff} \geq \frac{1}{2}\left|\vec{k} + \vec{G}\right|^2 \tag{3.15}$$

where $\vec{k}$ and $\vec{G}$ are respectively the reciprocal wave vector and lattice vector. The expression in Equation (3.15) arises from the fact that the contribution from the higher Fourier component in the Fourier expansion of the periodic system is negligible, thus allowing us to consider only the energy lower than this cutoff energy, $E_{cutoff.}$ A higher value of E_{curoff} implies including more plane wave basis for the calculation, thus representing a more accurate description of the total energy of the system.

3.8.2 *k*-points Mesh Convergence Tests

To accurately integrate the electronic properties of the system, it is vital to determine a sufficient number of *k*-points mesh for the calculation. A coarse *k*-points grid might result in the loss of continuity in the band structure leading to an inaccurate electronic- and optical-properties. The convergence test for *k*-points grid is carried out by incrementally increase the fineness of *k*-points using equilibrium lattice parameter determined in the previous section.

3.9 Summary

In summary, the concept of DFT is discussed in this chapter. The derivation of Kohn-Sham equation using Hohenberg-Kohn Theorem is discussed. The Quantum ESPRESSO simulation package is introduced in this chapter too. The concept of cutoff energy, cutoff *k*-points are also discussed.

CHAPTER 4: RESULTS AND DISCUSSION

In this chapter, the computational results with detailed discussions are presented. Firstly, the structural and electronic properties of 2D Mg_2C, including the lattice parameter, buckling height are shown, followed by the energy band structure and density of states of 2D Mg_2C that adsorbed with the Li, Na, K and Ca adatoms. The anode material study was systematically carried out and presented here. This study begins with the identification of the preferred adsorption of Li, Na, K or Ca adatoms on the high-symmetry sites of 2D Mg_2C. The diffusion profile of the adatoms on 2D Mg_2C is subsequently determined, followed by calculation of the theoretical specific capacity. A comparison of the specific capacity and diffusion energy with other anode materials is carried out and summarized in Figure 4.12. Finally, the convex hull and open-circuit voltage (OCV) are calculated. Key results of the present study have been published in the Journal of Physics: Condensed Matter (Chu et al., 2021).

4.1 Convergence Tests

To begin with the computational study using DFT, a convergence test was carried out in the first place. It is in our best interest to carry out the calculation with a lower computational cost, i.e., shortest computation time and lowest computational resource (memory consumed) without losing the accuracy of the calculation result. The purpose of the convergence test is to identify the smallest possible value for cutoff energy and *k*-point such that the computational work could be achieved in a timely manner while conserving the accuracy. The following section presents the cutoff energy convergence

test and the *k*-point test.

4.1.1 Cutoff Energy Convergence

In the cutoff energy convergence test, a variation of cutoff energy from 5 to 100 Ry is employed to obtain the total energy. The result is presented in Figure 4.1. The total energy of the 2D Mg_2C system gradually decreases from 5 Ry to 30 Ry. The energy decreases due to the additional plane wave basis being included into the calculation of the total energy, yielding a more accurate description of the total energy. A converging trend is observed when the cutoff energy is further increased from 30 Ry to 100 Ry, i.e., the total energies obtained do not vary with respect to the increasing cut off energy. In principle, a higher cutoff energy will give rise to a result with higher accuracy. Needless to say, the tradeoff for that is the higher computing cost and time required. Thus, in practice for all DFT calculations, a cutoff energy that is sufficiently high is good enough for obtaining results to an adequate degree of accuracy. Thus, from Figure 4.1, a cutoff energy of 40 Ry is adopted in further calculations.

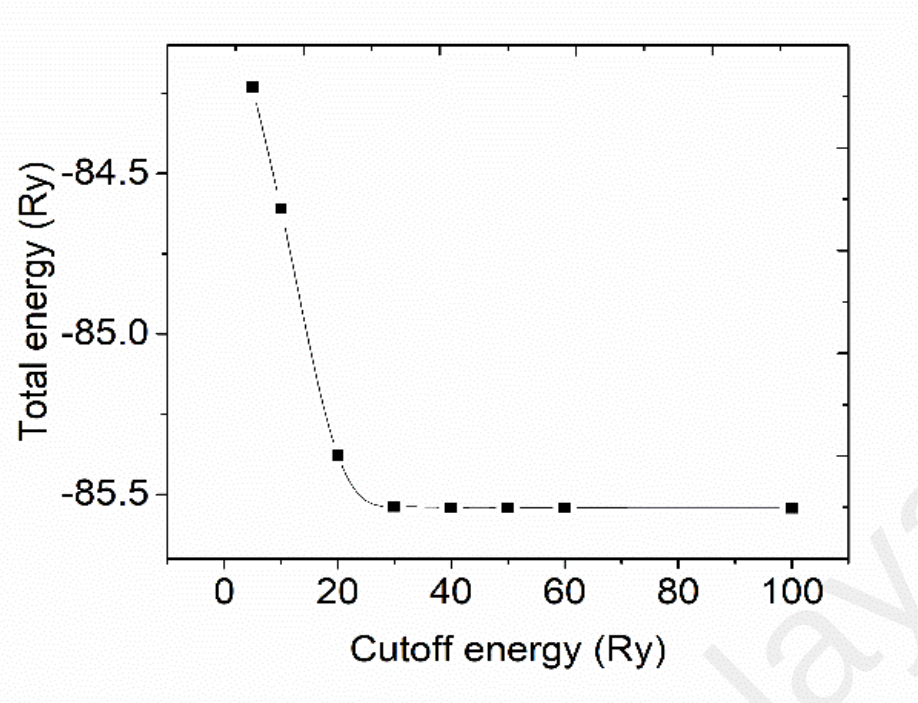

Figure 4.1: Total energy as a function of cutoff energy.

4.1.2 K-point Convergence

Figure 4.2 shows the total energy with respect to different number of *k*-point grids. Since 2D Mg_2C is a two-dimensional system, the corresponding *k*-point grids in the calculations are taken as $n \times n \times 1$, with the number of grids in the z-direction taken as 1 to represent the 2D nature of the system. Similar to the case of cutoff energy convergence, the total energy decreases gradually with the increasing fineness of the *k*-point mesh. This is because as the *k*-point mesh is denser, it provides a more accurate description of total energy in the first Brillouin zone of the reciprocal space. The convergence has achieved when the *k*-point grid is $5 \times 5 \times 1$, i.e., the total energies obtained do not vary with the increasing finest of the *k*-point grids. Hence, for all calculations, a *k*-point grid of $5 \times 5 \times 1$ is sufficient except for the energy band and density of states calculations, which requires

a *k*-point grid of 15 × 15 × 1. This is because for SCF calculations, the periodicity of the system is considered by sampling the *k*-points in the Brillouin zone. However, in the band structure and DOS calculations, it involves the electron densities along the path of *k*-points in the Brillouin zone. Thus, a finer *k*-point mesh would better illustrate the change in the electron densities along each path.

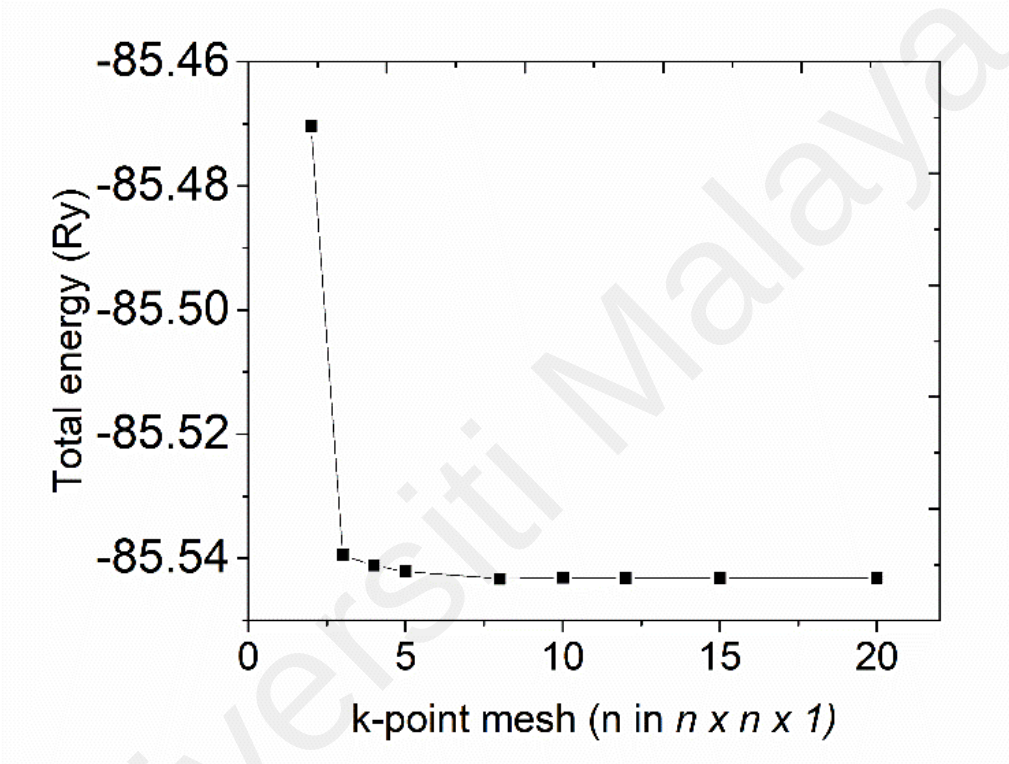

Figure 4.2: Total energy against k-point mesh.

4.2 Optimized Structure of 2D Mg_2C

In this project, the projector-augmented-wave (PAW) pseudopotential was adopted throughout all calculations to consider the electron-ion interactions. The calculation was carried out using generalized gradient approximation (GGA) with the Perdew–Burke–Ernzerhof (PBE) exchange correlation functional (Perdew et al., 1996a). The kinetic energy cutoff for the plane-wave basis and charge density cutoff was set to 40 and 280 Ry,

respectively. A 20 Å vacuum layer was included perpendicular to the 2D material to prevent the interlayer interaction. Structural relaxations were carried out until the interatomic force is less than 10^{-4} Ry/a.u. For the energy band and density of states (DOS) calculations, Brillouin zone was sampled using a Monkhorst−Pack grid of $15 \times 15 \times 1$ while for all other calculations, the momentum space was sampled on a coarser k-mesh of $5 \times 5 \times 1$.

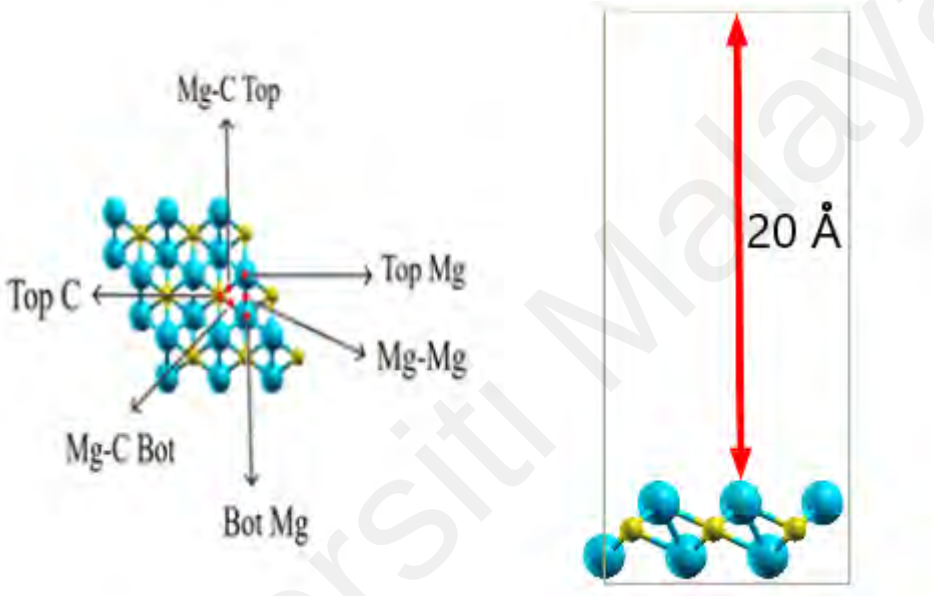

Figure 4.3: Top view of a 2D Mg_2C supercell, consisting of six high-symmetry sites denote as top C, top Mg, bot Mg, Mg–C bot, Mg–C top and Mg–Mg. A 20 Å vacuum layer was inserted to prevent interlayer interaction. Yellow balls denote C atoms, while blue balls denote Mg atoms.

The 2D Mg_2C has been reported to be in a morphology of hexagonal honeycomb structure. Before moving into the anode material study, we have to first verify the validity of the reported parameters employed in our calculation. Firstly, the optimization of the crystal structure of a free-standing 2D Mg_2C using the *vc-relax* flag in the Quantum ESPRESSO input was carried out. The relaxation is achieved when interatomic force is less than 10^{-4} Ry/a.u.

There are three atoms in a unit cell of 2D Mg_2C, where one carbon atom is connected to two magnesium atoms located on top and bottom of it respectively, forming a quasi-planar plane with a buckling height (Δ) of 1.86 Å as shown in Figure 4.4. The lattice parameters are $a = b = 3.54$ Å, whereas the calculated Mg-C-Mg bond angle, C-Mg and Mg-Mg bond length are 66.49°, 1.78 Å and 1.95 Å, respectively. All these parameters are close to those reported in the literature (Naseri, 2017; Meng et al., 2017; Wang et al., 2018). This structure is similar to that of another recently reported 2D material, 2D Be_2C, where the magnesium atoms are replaced by beryllium atoms. This morphology of carbide-based 2D material, where a quasi-planar structure consisting metal atoms sandwiching a carbon atom could potentially be another class of 2D material family to be further investigated.

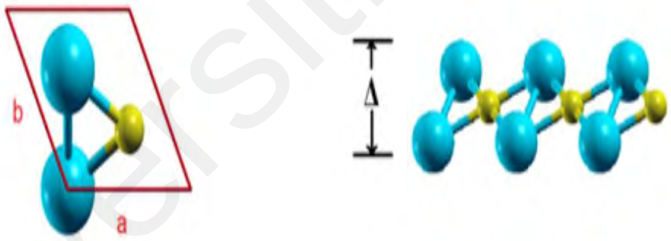

Figure 4.4: Crystal structure of 2D Mg_2C. *a*, *b*, and Δ are lattice parameters and buckling height of 2D Mg_2C respectively. Yellow balls denote C atoms, while blue balls denote Mg atoms.

4.3 Energy Band Diagrams and Density of States (DOS)

To study the effect of adatoms on the electronic structures of 2D Mg_2C, the energy band diagram and density of states (DOS) of the 2D Mg_2C adsorbed with Li, Na, K or Ca adatoms are plotted and presented in Figure 4.5. It is observed that the metallicity of the 2D Mg_2C is enhanced with the adatoms adsorption as evidenced by the presence of DOS in the Fermi level. It implies the overlapping of the valence and conduction band such that there

exist electrons in these states that are thermally active and could contribute to the conduction. In contrast, for an insulator or semiconductor, the Fermi level is located somewhere between the band gap, and the DOS would be zero, i.e., no electrons occupy the energy level in the band gap. In Figure 4.5, it is shown that higher DOS is found at the Fermi level of Na and K adsorbed systems than that of the Li and Ca adsorbed system. This shows that more states are available for electron occupation at the Fermi level and thus could provide better conductivity as there are more thermally active electrons. In the anode material study, the metallicity of an anode material is undoubtedly beneficial to the conductivity of the adatoms.

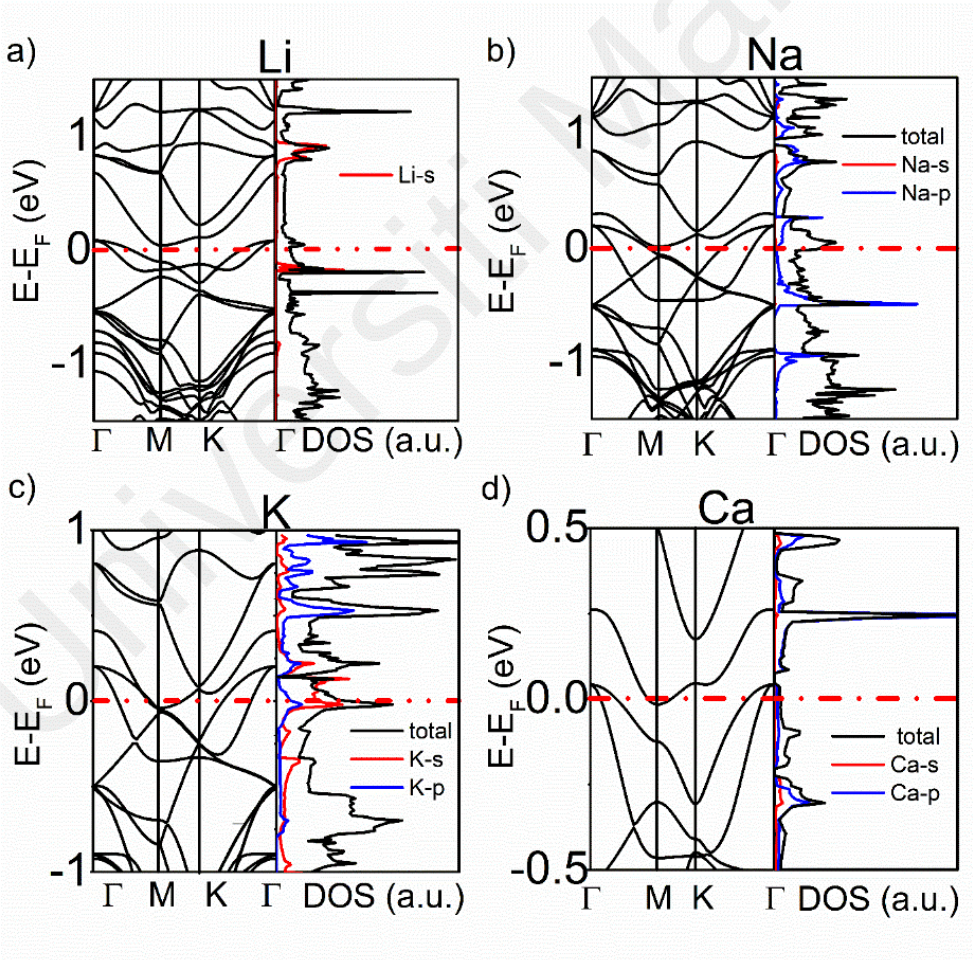

Figure 4.5: Energy band diagrams and density of states (DOS) of a 2D Mg_2C adsorbed with (a) Li (b) Na (c) K and (d) Ca adatoms. Red dashed lines denote the normalized Fermi energy level, E_F.

4.4 Preferable Adsorption Sites and Binding Energies

The binding energy is determined by:

$$E_{\mathrm{B}} = E_{Mg_2C+x} - E_{Mg_2C} - E_x \tag{4.1}$$

where E_{Mg_2C+x} and E_{Mg_2C} are the total energy of the optimized 2D Mg_2C adsorbed with the adatoms where *x* represents Li, Na, K or Ca, and the energy of the pristine 2D Mg_2C, respectively. E_x is energy of the Li, Na, K or Ca that calculated using the same supercell parameters as the 2D Mg_2C. The most preferred adsorption site corresponds to the one with the lowest E_B. Generally, a stable structure should have a binding energy of a negative value. The greater the binding energy (absolute value), the more stable the structure is. Thus, the preferred adatoms (Li, Na, K or Na) adsorption site is found by checking whichever site corresponds to the greatest (absolute value) binding energy.

In the anode material study, first we need to identify the preferable adsorption sites of the adatoms on the surface of the materials of interest and the stability of the system upon adsorption of the adatoms. Due to the morphology identical to that of the 2D Be_2C (Li et al., 2014; Naseri et al., 2018), 2D Mg_2C also has six possible adsorption sites as shown in Figure 4.6. The possible adsorption sites, and the notation are summarized in Table 4.1. These notations will be used throughout this dissertation.

Table 4.1: Notation of adsorption site.

Location	Description	Notation
a	On top of the Mg atom in the lower atomic plane	Bot Mg
b	On top of the Mg atom in the upper atomic plane	Top Mg
c	On top of the C atom	Top C
d	On top of the Mg-Mg bond	Mg-Mg
e	On top of the bond between the lower Mg and C	Mg-C bot
f	On top of the bond between the upper Mg and C	Mg-C top

To determine the most preferred adsorption site for the adatoms, a single Li Na, K or Ca atom was placed on each of the high-symmetry adsorption sites for a 3×3 2D Mg_2C supercell as indicated in Figure 4.6 and Table 4.1 followed by relaxations of atomic positions and cell parameters. Note that the final adsorption site does not necessarily be the same as the initial adsorption site, i.e., the adatoms would diffuse and adsorb to the site that corresponds to the minimum binding energy. The objective is to verify the most stable adsorption site(s) with the minimum energy. However, if the binding energy relative to the Top C (i.e. the most stable adsorption site) is lower than the thermal excitation energy (~26 meV), it could migrate between these sites. Using Equation 4.1, the binding energies are calculated. The initial, final adsorption site, binding energy and energy relative to Top C are calculated and summarized in Table 4.2.

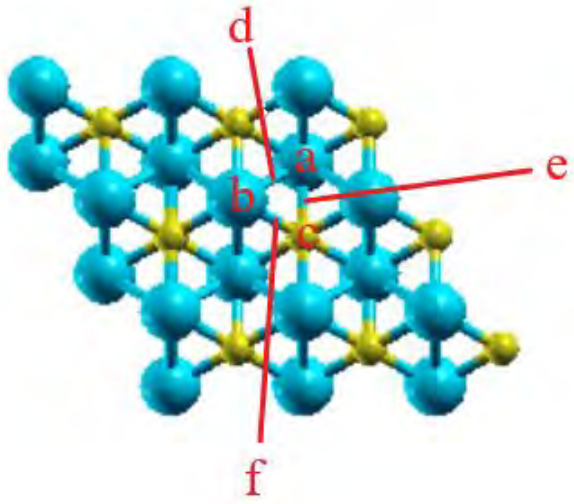

Figure 4.6: Top view of a 2D Mg_2C supercell, consisting of six high-symmetry sites denote as Top C, Top Mg, Bot Mg, Mg-C bot, Mg-C top and Mg-Mg. Yellow balls denote C atoms, while blue balls denote Mg atoms.

Table 4.2: Absorption position of metal ions on 2D Mg_2C, binding energy and total energy relative to the Top C site. Highlighted box denotes the preferred adsorption site(s).

a) Li adsorption

Initial Li position	Final Li position	Binding energy, E_b(eV)	Energy relative to the Top C (meV)
Bot Mg	Bot Mg	-1.1908091	758.4301
Top C	Top C	-1.9491039	0.13532
Mg-C Top	Top C	-1.9492392	-
Mg-C Bot	Top C	-1.9472080	2.03116
Mg-Mg	Bot Mg	-1.1903429	758.8963
Top Mg	Top Mg	-1.0783500	870.8892

Table 4.2, continued

b) Na adsorption

Initial Na position	Final Na position	Binding energy, E_b(eV)	Energy relative to the Top C (meV)
Bot Mg	Bot Mg	-0.9980216	3.232584
Top C	Top C	-1.0012542	-
Mg-C Top	Top C	-1.0007266	-
Mg-C Bot	Top C	-0.5304749	470.779232
Mg-Mg	Bot Mg	-0.998188	3.06612
Top Mg	Top Mg	-0.9199989	81.25524

c) K adsorption

Initial K position	Final K position	Binding energy, E_b(eV)	Energy relative to the Top C (meV)
Bot Mg	Bot Mg	-0.2678408	-
Top C	Top C	-0.2750692	-
Mg-C Bot	Top C	-0.2750706	-
Mg-C Top	Top C	-0.2750649	-
Mg-Mg	Bot Mg	-0.267849	-
Top Mg	TopMg	-0.1917522	83.3184

d) Ca adsorption

Initial Ca position	Final Ca position	Binding energy, E_b(eV)	Energy relative to the Top C (meV)
Bot Mg	Bot Mg	-0.5504556	87.47
Top C	Top C	-0.6379299	-
C-Mg Bot	Top C	-0.6392604	-
C-Mg Top	Top C	-0.6389474	-
Mg-Mg	Bot Mg	-0.5502	87.47
Top Mg	Top Mg	-0.3834292	255.83

Table 4.2 shows the final adsorption site and the corresponding binding energy. The energy difference is computed by taking the difference between the lowest binding energy value and the respective binding energy. It is interesting to see that for all the cases the adatoms would eventually diffuse to the Top C, as it became the most stable adsorption site. In Table 4.2(a), there exists three final adsorption sites, namely the Top C, Bot Mg and Top Mg sites. However, only the Top C has the lowest binding energy (-1.94 eV), whereas the binding energy at other adsorption sites are considerably larger than that (~700-800 meV). Thus, we can conclude that the preferable adsorption site for the Li adsorption on 2D Mg_2C is the Top C position. The preferred adsorption sites are summarized in Table 4.2.

In Table 4.2(b), the lowest binding energy (-1 eV) corresponds to the Top C adsorption site. The binding energy of a Li ion absorbs at the Bot Mg site is -0.998 eV, with a difference of merely 3 meV. Hence, it should also be considered as preferred adsorption site other than the Top C site. Similarly, K adsorption has also two preferable adsorption sites (Top C, Bot Mg). For comparison, the preferred adsorption site for Li or Ca adatom is the Top C with binding energy of -1.95 and -2.05 eV, respectively. For Na and K, the corresponding adsorption sites are the Top C and Bot Mg, with binding energy of -1 and -0.87 eV, respectively. All the calculated E_B upon the adsorptions of the adatoms have a negative value, suggesting that the adatom adsorptions are energetically stable.

4.5 Diffusion Profile and Energy Barrier

To study how well an adatom can diffuse on the surface of 2D Mg_2C, we can calculate the diffusion energy. There are six high-symmetry sites for the 2D Mg_2C morphology, as shown in Figure 4.6. These high-symmetry sites are denoted as Mg-C Top, Top C, Mg-C Bot, Bot Mg, Top Mg and Mg-Mg. To calculate the diffusion path, first, the initial and final states were identified by calculating the binding energy on those sites. The most preferable adsorption sites are then set as the initial and final states. The Li, Na, K or Ca adatom was set to diffuse along these high symmetry line between two neighboring preferred adsorption sites as determined previously. The diffusion pathway was calculated by using the climbing-image nudged elastic band (CI-NEB) (Henkelman & Jónsson, 2000). A total of six intermediate images were obtained through linear interpolation along the reaction path between the initial and final states for the diffusion pathway calculation. Then, relaxation was performed on these atomic coordinates until the force orthogonal to the path was less than 0.05 eV/Å.

Since the diffusion energy significantly dictates the charge and discharge rate of the NIBs, LIBs, KIBs or CIBs system, the diffusion barrier should be low such that the migration of the ions can occur easily. The Na, Li, K or Ca adatom was set to diffuse along the high symmetry line between two neighboring preferred adsorption sites on the 2D Mg_2C as shown in Figure 4.7. Since the Na or K adatom has two possible adsorption sites, there are three possible diffusion pathways, i.e. from the Bot Mg to Bot Mg, Top C to Bot Mg and Top C to Top C. From the energy profiles obtained via the NEB calculation (Figure 4.8), the energy barrier for Li diffusion is 0.7 eV. For the case of Na, the estimated energy barrier is 0.08 eV along the C-C and Mg-

Mg directions. However, the calculated diffusion barrier along the C-Mg direction is 0.06 eV lower than energy profile value of C-C. Similarly, for the case of K, the estimated barrier is 0.043 eV along C-C and Mg-Mg direction and 0.01 eV for diffusion along C-Mg direction. As for Ca, the diffusion barrier is computed to be 0.9 eV, which is the highest among all the cases. In Figure 4.8 (b) and (c), it is noticed that since there are two preferable adsorption sites for both Na and K adatoms, the diffusion of Na or K adatoms to these neighbouring sites (C-Mg) would require significantly lower energy as they are diffused between the lowest energy sites. A low diffusion barrier indicates that the adatoms could diffuse easily from one site to another. In the charge-discharge process, low diffusion barrier would lead to an easier diffusion process and thus, could significantly increase the charge-discharge rate. For both Na and K, the diffusion barrier is nearly an order of magnitude lower than that of Li suggesting that Mg_2C is a promising anode material for both the NIBs and KIBs.

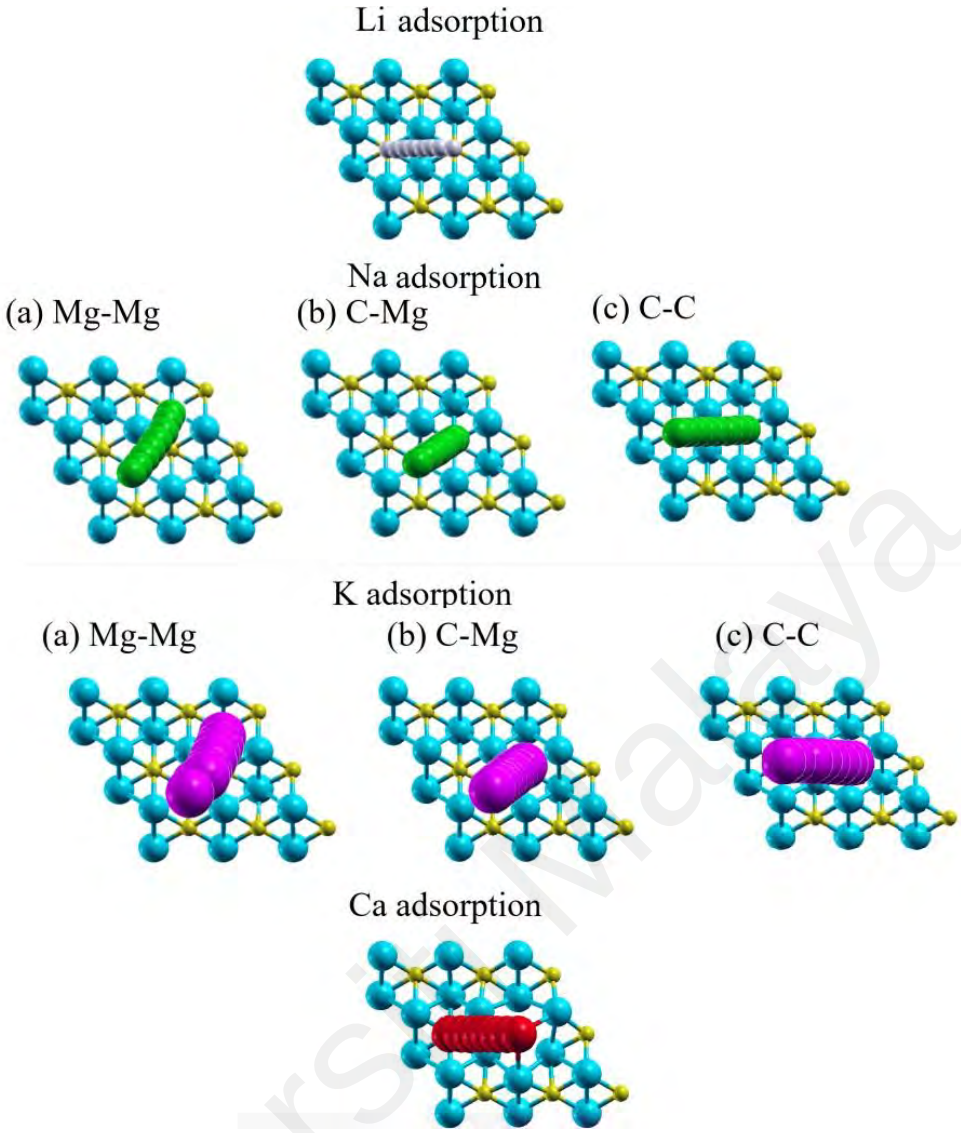

Figure 4.7: Diffusion paths for the Li, Na, K and Ca adsorptions on a 2D Mg_2C. Grey, green, purple and red balls denote the Li, Na, K and Ca atoms, respectively.

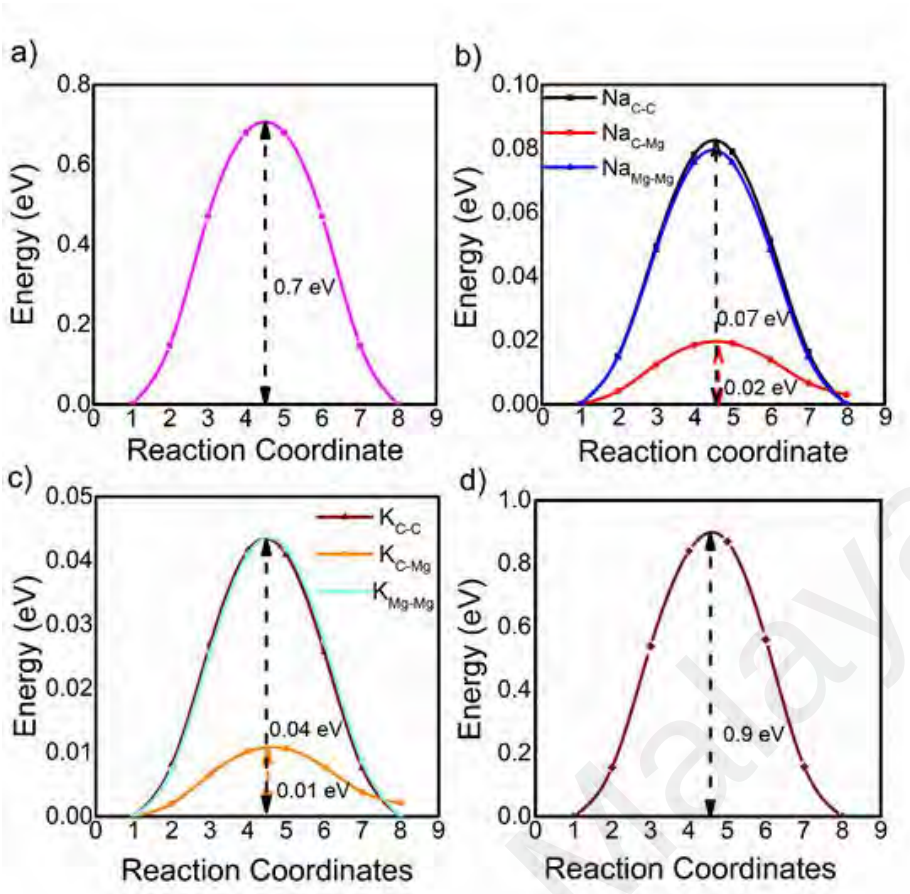

Figure 4.8: Diffusion profiles of (a) Li (b) Na (c) K and (d)Ca on 2D Mg_2C.

A very crucial parameter in anode material application is the theoretical specific capacity. For an anode application, it is desirable to have as high storage capacity as possible. This could be achieved in two ways: increasing the storage of adatoms in the anode system or utilizing ions with more charges. This is demonstrated in Equation (4.2). In this section, we will discuss the maximum amount of adatoms (Li, Na, K or Ca) that can be adsorbed on the 2D Mg_2C, which will subsequently determine the theoretical specific capacity.

In order to determine the maximum amount of adatoms that can be adsorbed on 2D Mg_2C, a double-sided adsorption is carried out by placing two Li, Na, K or Ca adatoms on both sides of the 2D Mg_2C on the preferred

adsorption sites followed by the relaxation of the crystal structures. The double-sided adsorption represents the fully adsorbed anode material. In present work, the adatom concentrations is taken by considering 1×1, 2×1, 2×2, 3×2 and 3×3 supercells, which corresponds to the stoichiometry of x = 2, 1, 0.5, 0.33, 0.22, for Li and Ca, and x = 4, 2, 1, 0.67, 0.44 for Na and K, respectively. The stoichiometry is taken from the chemical formula of A_xMgC (A = Li, Na, K or Ca).

Due to the larger ionic radius of Na and K, it is expected that the adsorption of these atoms at a high concentration may results in large volumetric expansion, which could lead to a structural deformation. However, in this study, there were no obvious structural deformations for all cases of x = 0 to 4, except for the case of x = 1 calciation. Even when the Na of K adatom concentration is further increased to x = 4, no significant structural deformation is observed in the crystal structure (see Figure 4.9). The calculated volume changes of crystal structure upon the adatoms adsorption relative to the pristine 2D Mg_2C shows that the crystal structures were compressed upon adatoms adsorption, with the volume compression of 1.35%, 1.1%, 2.03% and 1.06% for the Li, Na, K and Ca adsorptions, respectively. Therefore, it is expected that there will be no bond breaking upon the adsorption of Li, Na or K adatoms.

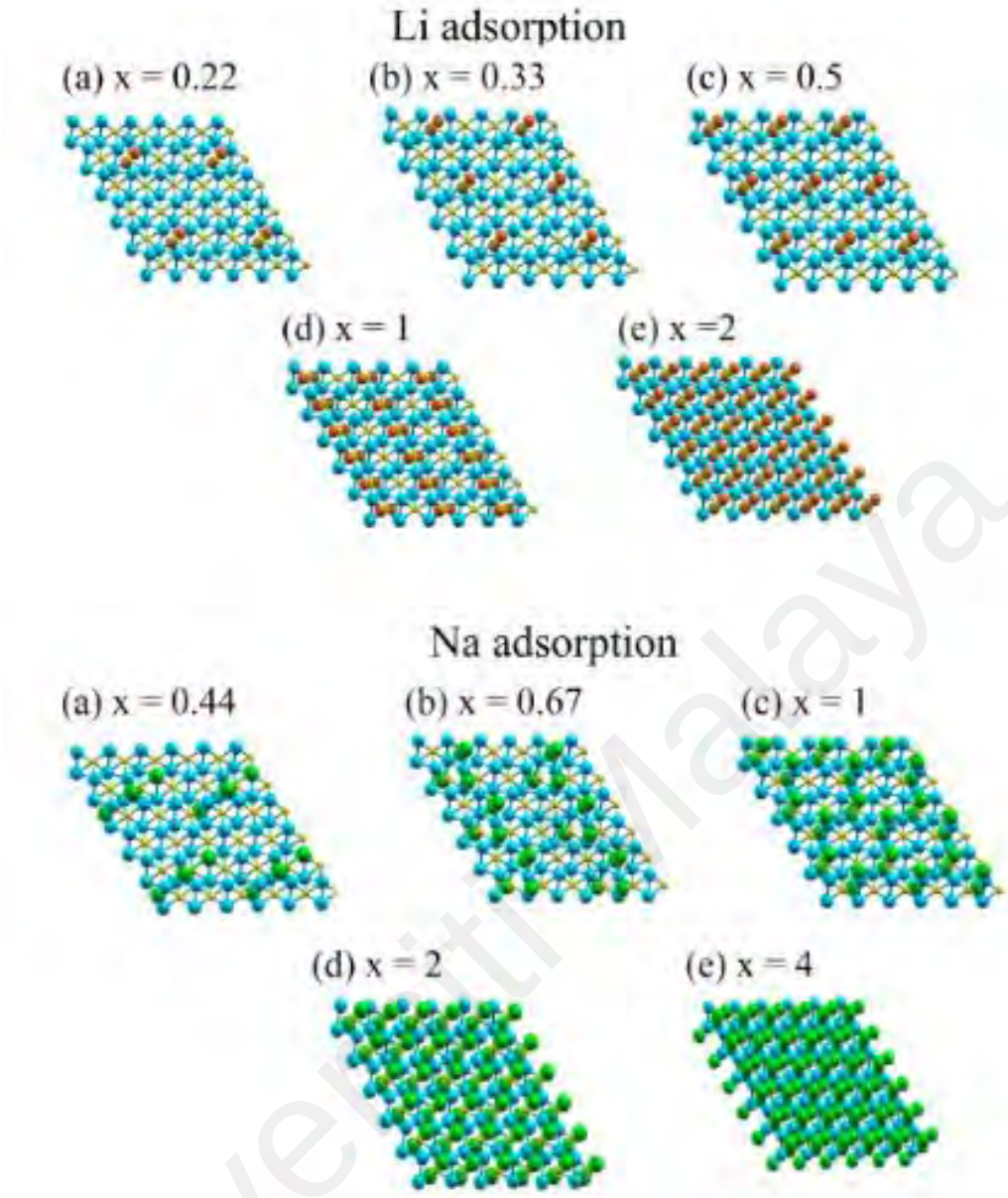

Figure 4.9: Atomic structures of the 2D Mg_2CLi, Mg_2CNa, Mg_2CK and Mg_2CCa with different concentrations. Orange, green, purple and red balls denote the Li, K, Na and Ca atoms, respectively.

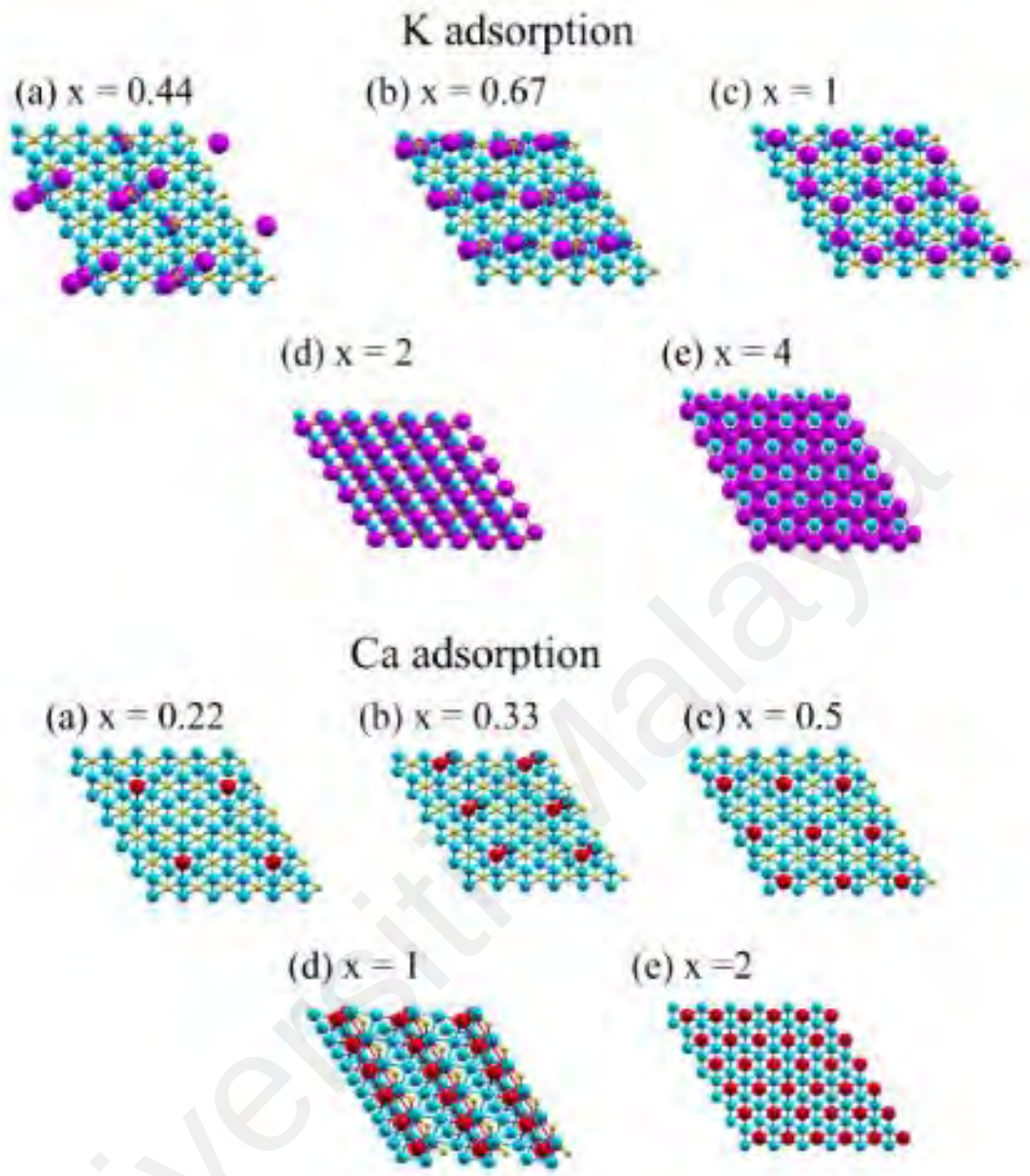

Figure 4.9, continued

4.6 Binding Energies Between Metal Ions and 2D Mg2C

The structural stability of the 2D Mg_2C adsorbed with adatoms with different stoichiometries can be further investigated by calculating the binding energy of adatoms at different concentrations. The calculated binding energy in Figure 4.10 are all negative values indicating the adsorption processes are exothermic. This ensures a good cycling stability if 2D Mg_2C were to be used as anode material for battery. Encouragingly, even at high

concentration of x = 4, the binding energy of Na(K) on the 2D Mg_2C is relatively high at -0.54 eV (-0.56 eV), suggesting the structural stability of 2D Mg_2C at high ionic concentration, yielding a greater theoretical specific capacity.

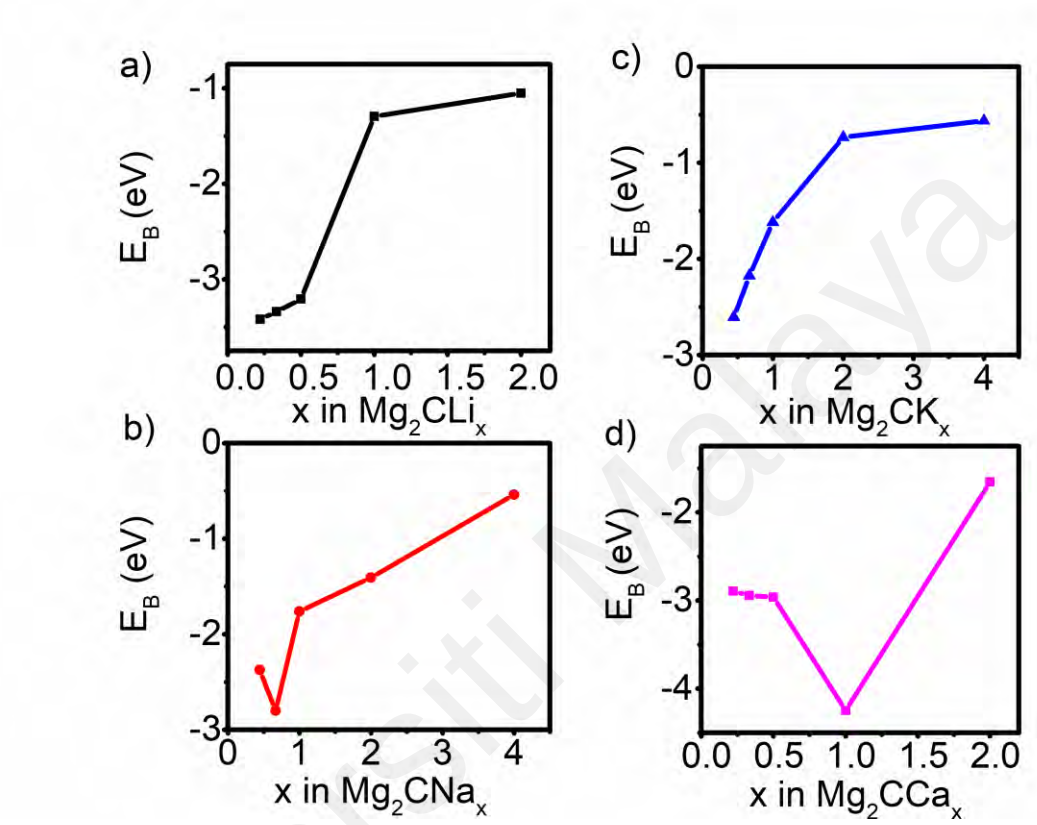

Figure 4.10: Binding energy profiles E_B as a function of (a) Li, (b) Na, (c) K and (d) Ca contents in 2D Mg_2C.

In Figure 4.10 the binding energy profile as a function of the Li, Na, K or Ca contents in 2D Mg_2C is plotted. Generally, the E_B becomes weaker when the adatom concentration is sufficiently high owing to the increasing coulombic repulsion as a result of increasing adatom, thus, leading to the increment of E_B. All the calculated E_B have negative values implying that the Li, Na or K adsorption on the 2D Mg_2C is energetically stable.

The study of adatoms adsorption on borophene (Khanifaev et al., 2017) and germanene (Pang et al., 2014) showed that at lower adatom concentration, the binding energy E_B is stronger due to larger charge transfer. However, at higher concentrations of adatoms, the increase in the electrostatic repulsions results in the weaker E_B. The E_B in 4.10(b) also follows the trend.

Notice that in Figure 4.10(d), the E_B with $x = 1$ is significantly larger, which reflects the strong binding of the Ca adatom with the 2D Mg_2C in a 2 × 1 cell. When we further investigate the structure of a double-sided adsorption 2D Mg_2C in a 2 × 1 cell, the structure is slightly deformed. This could be the reason for the steep drop in the binding energy. Thus, at this stage the suitability of 2D Mg_2C as CIBs is questioned owing to its possible structural instability. Generally, the strength of the Columbic repulsion and charge transfer are the factors that affect the strength of E_B. We will further discuss other properties to examine the feasibility of 2D Mg_2C based on the overall performance.

Thus, in conclusion, the maximum Li and Ca that can be adsorbed on 2D Mg_2C is $x_{max} = 2$ while for Na and K is $x_{max} = 4$.

4.7 Theoretical Specific Capacity

The maximum theoretical specific Li, Na, K or Ca storage, capacity C_M, is calculated as:

$$C_{\mathrm{M}} = \frac{1}{M_{Mg_2C}}(z \times x_{max} \times F \times 1000) \qquad (4.2)$$

where M_{Mg_2C} is the atomic mass of 2D Mg_2C, x_{max} is the maximum amount of Li, Na, K or Ca atom that can be adsorbed per unit formula of 2D Mg_2C, F is the Faraday constant = 26.81 Ah/mol and z is the valence number of the

adatom.

Now, we can calculate the theoretical specific capacity using Equation (4.2) with the x_{max} obtained from the previous section. For Li, Na and K, the valence electrons, z = 1 while z = 2 for Ca. With the same x_{max} and z, the maximum Na and K capacity can be estimated as 1770 mAhg^{-1}. As for Li and Ca, the maximum capacity is calculated to be 885 mAhg^{-1}. As discussed in Chapter 1, the conventional graphite anode material delivers a capacity of merely 372 mAhg^{-1}. In this study, the computed storage capacities are much higher than that of the graphite, with two times (LIBs, CIBs) and 4-fold (NIBs, KIBs) larger than LIBs using graphite. Moreover, the computed theoretical specific capacity of 2D Mg_2C as LIBs, NIBs, KIBs and CIBs are higher, if not comparable to various 2D materials, as shown in Section 4.10. This suggests that 2D Mg_2C is a promising candidate as anode materials.

4.8 Open-Circuit Voltage (OCV)

The charge/discharge process of a LIBs, NIBs, KIBs or CIBs follows a half-cell reaction that can be described by the following electrochemical process:

$$Mg_2C + xA^+ + xe^- \leftrightarrow Mg_2CA_x \qquad (4.3)$$

where A is Li, Na, K or Ca ion. By neglecting the volume and entropy effects, the average OCV can be estimated as:

$$\mathrm{OCV} \approx -\frac{E_{Mg_2\mathrm{CLi(Na/K/Ca)}_x} - E_{Mg_2\mathrm{C}} - xE_{\mathrm{Li(Na/K/Ca)(s)}}}{xe} \qquad (4.4)$$

where $E_{Mg_2CLi(Na/K/Ca)_x}$ and E_{Mg_2C} denote the fully lithated, sodiated, potassiated or calciated and pristine monolayer. $E_{Li(Na/K/Ca)(s)}$ is the energy of a single Li, Na, K or Ca atom defined using the similar method as proposed by Fan et al. (2013) and Yeoh et al (2019).

The applicability of the 2D Mg_2C as an anode material for battery can be further evaluated by calculating the average open-circuit voltage (OCV) using Equation (4.4). The average OCV is calculated to be 0.37, 0.50, 0.03 and 0.06 eV for LIBs, NIBs, KIBs and CIBs, respectively.

To further study the voltage profile, the voltage curve of the 2D Mg_2C battery system corresponding to different ionic concentration are plotted to give a better picture of the battery performance. The thermodynamically stable phases, also known as the metastable phases of 2D Mg_2C adsorbed with Li, Na, K or Ca are determined by constructing a convex hull. The formation energy with respect to each stoichiometry, *x* is calculated by:

$$E_f = E_{Mg_2\mathrm{CLi(Ca)}_x} - [\frac{x}{2}E_{Mg_2\mathrm{CLi(Ca)}_2} + \left(1 - \frac{x}{2}\right)E_{Mg_2C}]$$
$$E_f = E_{Mg_2\mathrm{CNa(K)}_x} - [\frac{x}{4}E_{Mg_2\mathrm{CNa(K)}_4} + \left(1 - \frac{x}{4}\right)E_{Mg_2C}] \quad (4.5)$$

where $E_{Mg_2\mathrm{CLi(Ca)}_x}$, $E_{Mg_2\mathrm{CLi(Ca)}_2}$ and E_{Mg_2C} are respectively the total energy of $Li(Ca)_xMg_2C$, fully lithiated (calciated) 2D Mg_2C and monolayer Mg_2C, and $E_{Mg_2\mathrm{CNa(K)}_x}$ and $E_{Mg_2\mathrm{CNa(K)}_4}$ are respectively the total energy of $Na(K)_xMg_2C$, fully sodiated (potassiated) 2D Mg_2C. Figure 4.11 shows the convex hull of 2D Mg_2C adsorbed with Li, Na, K or Ca with different concentrations. The thermodynamically stable intermediate phases of Li_xMg_2C, Na_xMg_2C, K_xMg_2C and Ca_xMg_2C are at x = 0.00, 0.22 and 2.00, x = 0.00, 2.00 and 4.00, x = 0.00, 0.67, 1.00, 2.00 and 4.00, x = 0.00, 1.00

and 2.00, respectively. These stoichiometries are then used to compute the voltage profile. From Figure 4.11, it is noticed that the voltage profile for K_xMg_2C is more favourable for anode application with its long plateaus shape instead of the large voltage steps as observed for the case for Li_xMg_2C, Na_xMg_2C and Ca_xMg_2C.

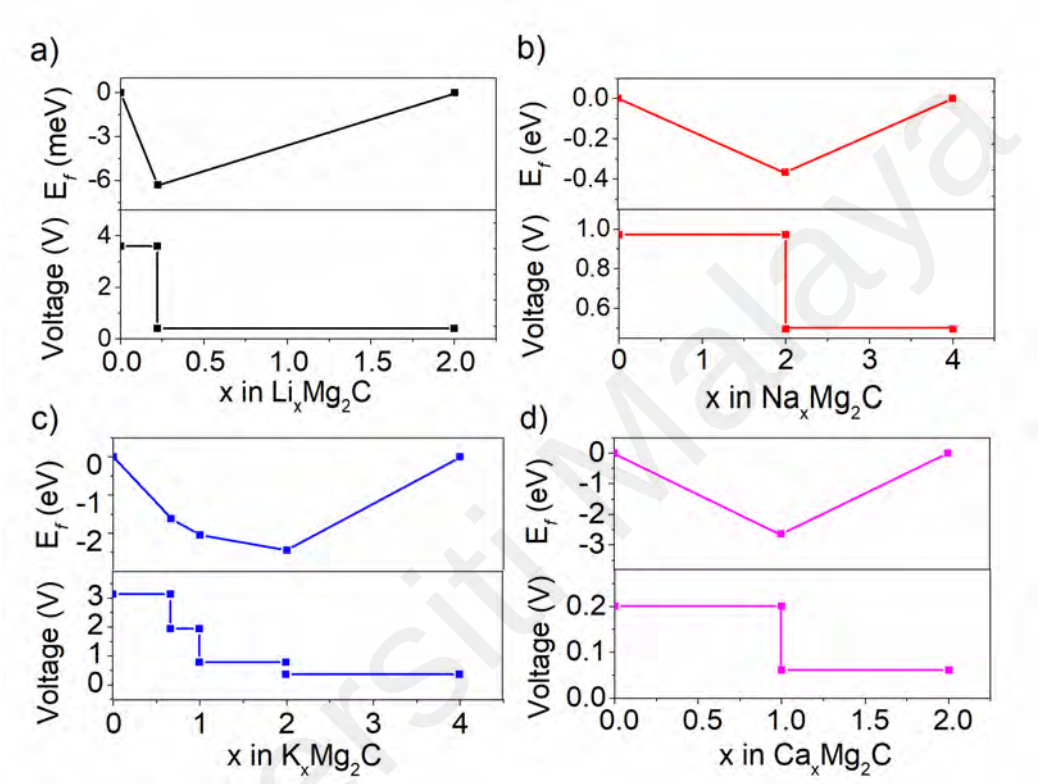

Figure 4.11: Energy convex hull and voltage profile for (a) Li_xMg_2C (b) Na_xMg_2C (c) K_xMg_2C and (d) Ca_xMg_2C with different stoichiometries.

4.9 Comparison of Specific Capacities and Diffusion Barriers

Figure 4.11 shows the comparison on the theoretical maximum capacity of Li, Na, K and Ca adatoms on a 2D Mg_2C as a function of diffusion barrier for various 2D materials. The present work on 2D Mg_2C is denoted as the red star. A material with high theoretical capacity and low diffusion barrier is considered an ideal anode material, i.e., the materials located at the upper left region of the figure. As shown in Figure 4.11, 2D

Mg_2C fulfills this criterion, especially for Na and K storage. Thus, we can consider 2D Mg_2C as a promising potential anode material for NIBs and KIBs. The specific capacity, diffusion barrier and OCV for Li, Na, K or Ca on 2D Mg_2C is summarized in Table 4.3.

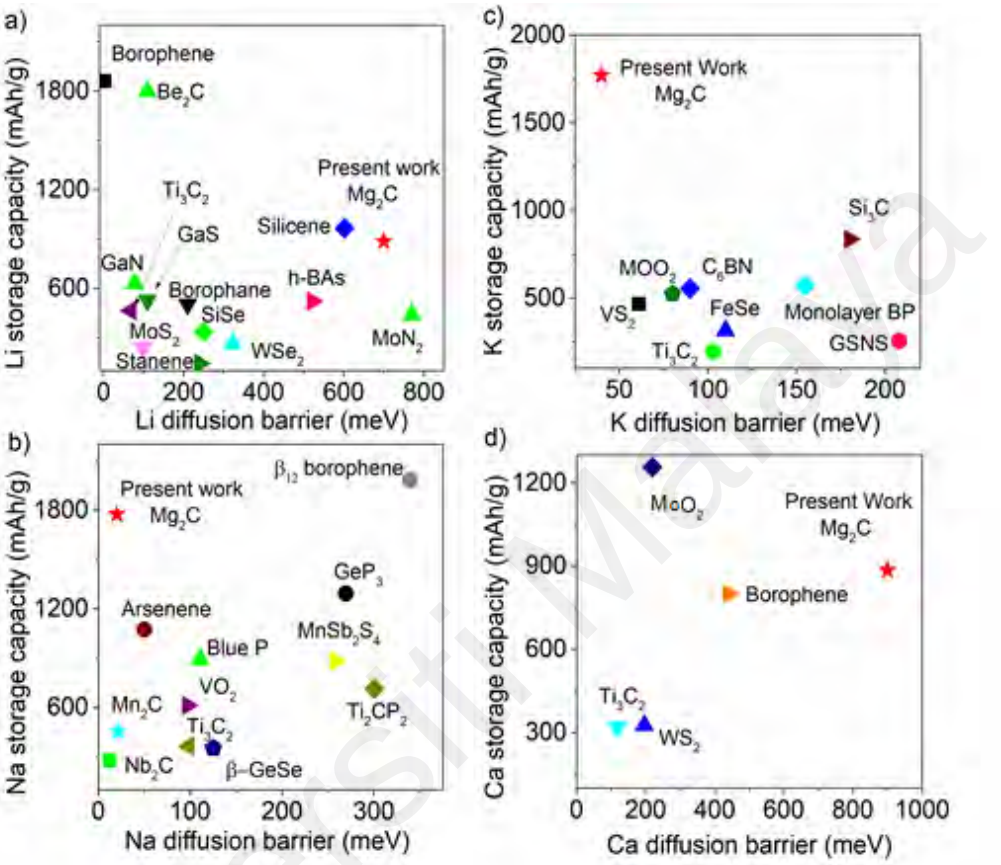

Figure 4.12: Comparison on the theoretical maximum capacity of (a) Li (b) Na (c) K and (d) Ca adatoms on a 2D Mg_2C as a function of diffusion barrier for various 2D materials.

Table 4.3: Specific capacity (C_M), diffusion barrier and OCV for Li, Na, K or Ca on 2D Mg_2C

	C_M ($mAhg^{-1}$)	Diffusion barrier (eV)	OCV (eV)
Li	885	0.70	0.37
Na	1770	0.08	0.50
K	1770	0.04	0.03
Ca	885	0.90	0.06

4.10 Summary

In summary, the convergence test was done before studying the anode material properties of 2D Mg_2C. It is sufficient to take the cutoff energy and *k*-point as 40 Ry and 5 × 5 × 1 in the calculation. Then, the optimization of cell parameters was performed to validate the data used for this study. The DOS and energy band structure was plotted and it is found that the 2D Mg_2C remains metallic upon adatom adsorptions. Next, the preferred adsorption sites and the corresponding binding energies are determined, where there is only one preferred adsorption site for Li, Ca (Top C) and two preferred adsorption sites for Na, K (Top C, Bot Mg).

After defining the preferred adsorption site, the migration of adatoms on 2D Mg_2C was studied using NEB calculation. The diffusion barrier was found to be the lowest for K diffusion with 0.04 eV. In Section 4.6-4.8, the maximum amount of adatom that can be adsorbed on 2D Mg_2C was determined and it is shown that the formation of Li_2Mg_2C, Na_4Mg_2C, K_4Mg_2C and Ca_2Mg_2C phases delivers a specific capacity of 885 $mAhg^{-1}$, 1770 $mAhg^{-1}$, 1770 $mAhg^{-1}$, 885 $mAhg^{-1}$ respectively. Finally, the OCV was calculated and discussed. The KIBs and CIBs exhibited the highest theoretical specific capacity, with a rather low diffusion barrier.

CHAPTER 5: CONCLUSIONS AND FUTURE WORK

This chapter concludes the present study and provides recommendation and improvement for future research.

5.1 Conclusion

Using first-principles DFT calculation, we have systematically studied the feasibility of 2D Mg_2C as anode material for metal ion batteries (LIBs, NIBs, KIBs and CIBs).

First, we introduced the motivation of exploring newly discovered 2D materials as anode materials. The graphite anode material suffers a low storage capacity. 2D materials can be an alternative to the conventional anode materials due to their unique morphology that could give rise to the high storage capacity. The alternative to LIBs has also been studied owing to the scarcity and pricy lithium salt to produce a high performing battery system. Combining these ideas, the search for alternative candidates anode materials of LIBs is the main objective of this research.

The study of anode materials for LIBs using DFT has been carried out systematically on 2D materials. In the present study, 2D Mg_2C has been chosen because of its exceptional electrical properties, particularly its metallicity upon external simulation. The research methodology employed in this study, i.e., DFT and the current development of anode materials from both theoretical and experimental point of view was also presented. Convergence tests were carefully carried out to verify the validity of the parameters adopted in our calculations before further studies were subsequently carried out. This ensures the calculated results are converged and resembles the true nature of the anode material system. It is found that the metallicity of 2D Mg_2C

retains with the adsorption of Li, Na, K or Ca adatoms, as a result, ensures a good electronic conductivity as battery electrodes. In addition, the calculated volume changes of ~1-2 % upon lithiation, sodiation and potassiation process has proven the structural stability of 2D Mg_2C.

Next, the calculation of diffusion barrier, a crucial parameter in determining the fast charge/discharge process was carried out. It is found that the diffusion of Na adatom on 2D Mg_2C exhibits a remarkable low diffusion barrier of 0.08 eV, which is nearly an order of magnitude lower than Li (0.7 eV). The diffusion barrier of K and Ca on 2D Mg_2C were 0.043 and 0.9 eV, respectively. For theoretical specific capacity calculation, it is concluded that 2D Mg_2C can provide stable adsorption to Li, Na, K or Ca up to Mg_2CLi_2, Mg_2CNa_4, Mg_2CK_4 or Mg_2CCa_2 with the maximum capacity for Li/Ca (Na/K) is of 884.52 $mAhg^{-1}$ (1770 $mAhg^{-1}$), which are exceptionally high for NIBs and KIBs applications. The calculated average OCV is low, i.e., 0.37 eV, 0.497 eV, 0.03 eV and 0.06 eV for LiB, NIBs, KIBs and CIBs respectively, suggesting the system is suitable for low charging voltage applications.

In this study of 2D anode material, an interesting correlation between the diffusion, storage properties and the ionic radii of the adatoms were observed. It is observed that the K-ion with the largest ionic radius has the lowest diffusion barrier of ~0.04 eV, while ions with a smaller radius has a higher diffusion barrier. This is due to the fact that the Li adsorption has a stronger binding energy with the 2D Mg_2C host of about -1.05 eV compared to the K adatom of -0.56 eV. For the storage properties, the 2D Mg_2C has higher storage capacity for Na- and K-ion, since it can host twice the number of

atoms for Na- and K- ions (larger ionic radii) as compared to that of Li-ion (smaller ionic radii). The divalent atom Ca was excluded from this comparative study of the ionic radii as it did not follow the trend.

5.2 Future Research

Although theoretical calculations predicted the structural stability of 2D Mg_2C (Meng et al., 2017; Naseri, 2017), the experimental synthesis mechanism still remains unknown. This poses a question concerning the degree of perturbation of intrinsic properties, especially the electrical properties of 2D Mg_2C. Thus, in this regard, it is suggested to conduct thorough theoretical calculation to screen for possible material that could potentially act as the substrate for the deposition of 2D Mg_2C without structural deformation. This could provide a reference for the experimental synthesis of 2D Mg_2C.

In addition, forming heterostructure with graphene or RGO layer (Shu et al., 2016) could enhance the structural stability during charge/discharge cycle and also improve the electrical conductivity. Besides that, few layer 2D materials are able to strengthen the material structure as observed in phosphorene (Xu et al., 2016). Thus, it is suggested to perform the anode material calculation on the 2D Mg_2C/graphene heterostructure or bilayer/few layer 2D Mg_2C to examine the changes in the anode material properties.

In this study, the research on multivalent ion battery was focused on CIBs. As the research on Al ion batteries remains largely unexplored (Gummow et al., 2018), it is a great opportunity to carry out DFT study on 2D Mg_2C as anode material for this trivalent ion battery.

5.3 Summary

By examining the adsorption site, diffusion barrier, capacity and OCV of 2D Mg_2C, it is concluded that the proposed material, 2D Mg_2C is a promising candidate for anode materials. Recommendation for future research includes the theoretical calculation to screen for possible substrate, for example, graphene, silicene or h-BN for 2D Mg_2C, calculating 2D Mg_2C/graphene heterostructure or bilayer/few layer 2D Mg_2C anode material properties and the study of Al ion batteries using 2D Mg_2C.

REFERENCES

Ai, W., Jiang, J., Zhu, J., Fan, Z., Wang, Y., Zhang, H., Huang, W., & Yu, T. (2015). Supramolecular polymerization promoted in situ fabrication of nitrogen-doped porous graphene sheets as anode materials for Li-ion battery. *Advance Energy Materials*, 5, Article#1500559.

Aydinol, M. K., Kohan, A. F., Ceder, G., Cho, K., & Joannopoulos, J. (1997). *Ab initio* study of lithium intercalation in metal oxides and metal dichalcogenides. *Physical Review B*, 56, 1354-1365.

Bang, G.S., Nam, K.W., Kim, J.Y., Shin, J., Choi, J.W., & Choi, S-Y. (2014). Effective liquid-phase exfoliation and sodium ion battery application of MoS_2 nanosheets. *ACS Applied Materials and Interfaces*, 6(10), 7084-7089.

Benzidi, H., Lakhal, M., Garara, M., Abdellaoui, M., El Kenz, A., Benyoussef, A., & Mounkachi, O. (2019). Arsenene monolayer as an outstanding anode material for (Li/Na/Mg) ion batteries: density functional theory. *Physical Chemistry Chemical Physics,* 21, 19951-19962

Chan, T. L., & Chelikowsky, J. R. (2010). Controlling Diffusion of Lithium in Silicon Nanostructures. *Nano Letters*, 10, 821−825.

Chen, X., Zheng, Y., Liu, W., Zhang, C., Li, S., & Li, J. (2019). High-performance sodium-ion batteries with a hard carbon anode: transition from the half-cell to full-cell perspective. *Nanoscale*, 11, 22196-22205.

Chu, Y. Z., Yeoh, K. H., & Chew, K.-H. (2021). A first-principles comparative study of lithium, sodium, potassium and calcium storage in two-dimensional Mg2C. *Journal of Physics: Condensed Matter,* 33, Article#075002.

Datta, M.K., Epur, R., Saha, P., Kadakia, K., Park, S.K., & Kumta, P.N. (2013). Tin and graphite based nanocomposites: Potential anode for sodium ion batteries. *Journal of Power Sources*, 225, 316-322.

David, L., Bhandavat, R., & Singh, G. (2014). MoS2/graphene composite paper for sodium-ion battery electrodes. *ACS Nano*, 8(2), 1759-1770.

D´avila, M., Xian, L., Cahangirov, S., Rubio A., & Le Lay, G. (2014). Germanene: a novel two-dimensional germanium allotrope akin to graphene and silicene. *New Journal of Physics*, 16, Article#095002.

Deng, X., Chen, X., Huang, Y., Xiao, B., & Du, H. (2019). Two-dimensional GeP3 as a high capacity anode material for non-lithium-ion batteries. *Journal of Physical Chemistry C*, 123, 8, 4721-4728.

Doron, A., Ella, Z., Yaron, C., & Hanan, T. (2002). A short review of failure mechanisms of lithium metal and lithiated graphite anodes in liquid electrolyte solutions. *Solid State Ionics*, 148, 405 – 416.

Dunn, B., Kamath, H., & Tarascon, J.-M. (2011). Electrical energy storage for the grid: a battery of choices. *Science*, 334, 928–935.

Er, D., Li, J., Naguib, M., Gogotsi, Y., & Shenoy, V. B. (2014). Ti_3C_2 MXene as a high capacity electrode material for metal (Li, Na, K, Ca) ion batteries. *ACS Applied Materials and Interfaces*, 6, 11173−11179.

Fan, X., Zheng, W. T., Kuo, J. –L., & Singh, D. J. (2013). Adsorption of single Li and the formation of small Li clusters on graphene for the anode of lithium-ion Batteries. *ACS Applied Materials and Interfaces,* 5, *7793-*7797.

Fjellvaag, H., & Karen, P. (1992). Crystal structure of magnesium sesquicarbide. *Inorganic Chemistry*, 31(15), 3260-3263.

Fong, R., von Sacken, U., & Dahn, J. R. (1990). Studies of lithium intercalation into carbons using nonaqueous electrochemical cells. *Journal of The Electrochemical Society,* 137(7), 2009-2013.

Gajdanowicz, P., Michard, E., Sandmann, M., Rocha, M., Correa, L. G. G., Ramirez-Aguilar, S. J. R., … Dreyer, I. (2010). Potassium (K+) gradients serve as a mobile energy source in plant vascular tissues. *Proceedings of the National Academy of Sciences of the United States of America,* 108(2), 864–869.

Giannozzi, P., Baroni, S., Bonini, N., Calandra, M., Car, R., Cavazzoni, C., … Wentzcovitch, R. M. (2009). QUANTUM ESPRESSO: a modular and open-source software project for quantum simulations of materials. *Journal of Physics: Condensed Matter,* 21, Article#395502.

Giannozzi, P., Andreussi, O., Brumme, T., Bunau, O., Buongiorno Nardelli, M., Calandra, M., … Baroni, S. (2017). Advanced capabilities for materials modelling with Quantum ESPRESSO. *Journal of Physics: Condensed Matter,* 29, Article#465901.

Goodenough, J.B., & Park, K-S. (2013). The Li-ion rechargeable battery: A perspective. *Journal of the American Chemical Society*, 135 (4), 1167-1176.

Gummow, R. J., Vamvounis, G., Kannan, M. B., & He, Y. (2018). Calcium-ion batteries: current state-of-the-art and future perspectives. *Advanced Materials*, 30, Article#1801702.

Hartree, D.R. (1928). The wave mechanics of an atom with a non-Coulomb central field. Part I. Theory and methods. *Mathematical Proceedings of the Cambridge Philosophical Society*, 24, 89-110.

Henkelman, G., & Jósson, H. (2000). Improved tangent estimate in the nudged elastic band method for finding minimum energy paths and saddle points. *Journal of Chemical. Physics*, 113, 9978-9985.

Hohenberg, P. & Kohn, W. (1964). Inhomogeneous electron gas. *Physical Review,* 136, B864-B871.

Hu, J., Xu, B., Ouyang, C., Zhang, Y., & Yang, S. (2016). A. Investigations on Nb_2C monolayer as promising anode material for Li or non-Li ion batteries from first principles calculations. *RSC Advances*, 6, 27467-27474.

Hwang, H., Kim, H., & Cho, J. (2011). MoS_2 nanoplates consisting of disordered graphene-like layers for high-rate lithium battery anode materials. *Nano Letters*, 11, 4826-4830.

Jana, S., Thomas, S., Lee, C. H., Jun, B., & Lee, S. U. (2019). B_3S monolayer: prediction of a high-performance anode material for lithium-ion batteries. *Journal of Materials Chemistry A*, 7, 12706-12712.

Jena, N.K., Araujo, R.B., Shukla, V., & Ahuja, R. (2017). Borophane as a benchmate of graphene: A potential 2D material for anode of Li and Na-ion batteries, *ACS Applied Materials & Interfaces*, 9, 16148-16158.

Jeong, G., Kim, Y.-U., Kim, H., Kim, Y.-J., & Sohn, H.-J. (2011). Prospective materials and applications for Li secondary batteries. *Energy & Environmental Science*, 4, 1986-2002.

Jian, Z., Luo, W., Ji, X. (2015). Carbon Electrodes for K-Ion Batteries. *Journal of the American Chemical Society,* 137(36), 11566-11569.

Jiang, H. R., Lu, Z., Wu, M., Ciucci, F., & Zhao, T. S. (2016). Borophene: A promising anode material offering high specific capacity and high rate capability for lithium-ion batteries. *Nano Energy*, 23, 97-104.

Jiang, H. R., Shyy, W., Liu, M., Wei, L., Wu, M. C., & Zhao, T. S. (2017). Boron phosphide monolayer as a potential anode material for alkali metal-based batteries. *Journal of Materials Chemistry A*, 5, 672-679.

Jing, Y., Zhou, Z., Cabrera, C. R., & Chen, Z. J. (2013). Metallic VS_2 monolayer: A promising 2D anode material for lithium ion batteries. *Physical Chemistry C*, 117, 25409−25413.

Karmakar, S., Chowdhury, C., & Datta, A. (2016). Two-dimensional group IV monochalcogenides: anode materials for Li-ion batteries. *Journal of Physical Chemistry C*, 120, 14522−14530.

Khanifaev, J., Peköz, R., Konuk, M., & Durgun, E. (2017). The interaction of halogen atoms and molecules with borophene. *Physical Chemistry Chemical. Physics*,19, 28963-28969.

Khossossi, N., Banerjee, A., Benhouria, Y., Essaoudi, I., Ainane, A., & Ahuja, R. (2019). Ab initio study of a 2D h-BAs monolayer: a promising anode material for alkali-metal ion batteries. *Physical Chemistry Chemical Physics*, 21, 18328-18337.

Kohn, W., & Sham, L. J. (1965). Self-consistent equations including exchange and correlation effects. *Physical Review*, 140, A1133-A1138.

Kokalj, A. (2003). Computer graphics and graphical user interfaces as tools in simulations of matter at the atomic scale. *Computational Materials Science*, 28, 155-168.

Komaba, S., Hasegawa, T., Dahbi, M., & Kubota, K. (2015). Potassium intercalation into graphite to realize high-voltage/high-power potassium-ion batteries and potassium-ion capacitors. *Electrochemistry Communications,* 60, 172–175.

Kubota, K., Dahbi, M., Hosaka, T., Kumakura, S., & Komaba, S. (2018). Towards K-ion and Na-ion batteries as "Beyond Li-ion". *Chemical Record,* 18, 459–479.

Lee, E., & Persson, K. A. (2012). Li absorption and intercalation in single layer graphene and few layer graphene by first principles. *Nano Letters*, 12, 4624−4628.

Lei, J. C., Zhang, X., & Zhou, Z. (2015). Recent advances in MXene: Preparation, properties, and applications. *Frontiers of Physics*, 10, 276–286.

Li, F., Qu, Y., & Zhao, M. (2016). Germanium sulfide nanosheet: A universal anode material for alkali metal ion batteries. *Journal of Materials Chemistry A*, 4, 8905-8912.

Li, Q., Yao, Z., Wu, J., Mitra, S., Hao, S., Sahu, T. S., Li, Y., Wolverton, C., & Dravid, V. P. (2017). Intermediate phases in sodium intercalation into MoS2 nanosheets and their implications for sodium-ion batteries. *Nano Energy*, 38, 342–349.

Li, W., Yang, Y., Zhang, G., & Zhang, Y.-W. (2015). Ultrafast and directional diffusion of lithium in phosphorene for high-performance lithium-ion battery. *Nano Letter,* 15(3), 1691-1697.

Li, Y., Liao, Y., & Chen. Z. (2014). Be_2C Monolayer with quasi-planar hexacoordinate carbons: A global minimum structure. *Angewandte Chemie International Edition*, 53, 1-6.

Li, Y., Wu, D., Zhou, Z., Cabrera, C. R., & Chen, Z. (2012). Enhanced Li adsorption and diffusion on MoS2 zigzag nanoribbons by edge effects: A computational study. *Journal of Physical Chemistry Letters*, 3, 2221–2227.

Liu, J., Zhang, C., Xu, L., & Ju, S. (2018). Borophene as a promising anode material for sodium-ion batteries with high capacity and high rate capability using DFT. *RSC Advances*, 8, 17773-17785.

Liu, H., Gao, G., Li, Y., Hao, J., & Tse, J.S. (2015). Crystal structures and chemical bonding of magnesium carbide at high pressure. *Journal of Physical Chemistry C*, 119(40), 23168-23174.

Lv, R., Robinson, J. A., Schaak, R. E., Sun, D., Sun, Y., Mallouk, T. E., & Terrones, M. (2014). Transition metal dichalcogenides and beyond: synthesis, properties, and applications of single- and few-layer nanosheets. *Accounts of Chemical Research*, 48(1), 56–64.

Lv, X., Wei, W., Sun, Q., Huang, B., & Dai, Y. (2017). A first-principles study of $NbSe_2$ monolayer as anode materials for rechargeable Lithium-ion and Sodium-ion batteries. *Journal of Physics D: Applied Physics*, 50, Article#235501.

Mannix, A. J., Zhou, X. F., Kiraly, B., Wood, J. D., Alducin, D., Myers, B. D., Liu, X., Fisher, B. L., Santiago, U., Guest, J. R., & Yacaman, M. J. (2015). Synthesis of borophenes: Anisotropic, two-dimensional boron polymorphs. *Science*, 350, 1513–1516.

Mashtalir, O., Naguib, M., Mochalin, V. N., Dall'Agnese, Y., Heon, M., Barsoum, M. W., & Gogotsi, Y. (2013). Intercalation and Delamination of Layered Carbides and Carbonitrides. *Nature Communications*, 4, Article#1716.

Meng, L., Ni, S., Zhou, M., Zhang, Y., Li, Z., & Wu, W. (2017). Metal-semiconductor transition of two-dimensional Mg2C monolayer induced by biaxial tensile strain. *Physical Chemistry Chemical Physics*, 19, 32086-32090.

Mizushima, K., Jones, P. C., Wiseman, P. J., & Goodenough, J. B. (1980). LixCoO2 (0<x<-1): A new cathode material for batteries of high energy density. *Materials Research Bulletin,* 15(6), 783-789.

Mortazavi, B., Dianat, A., Cuniberti, G., & Rabczuk, T. (2016). Application of silicene, germanene and stanene for Na or Li ion storage: A theoretical investigation. *Electrochimica Acta*, 213, 865–870.

Mortazavi, M., Wang, C., Deng, J., Shenoy, V. B., & Medhekar, N. V., (2014) Ab initio characterization of layered MoS2 as anode for sodium ion batteries. *Journal of Power Sources*, 268, 279–286.

Mukherjee, S., Kavalsky, L., & Singh, C. V. (2018). Ultrahigh storage and fast diffusion of Na and K in blue phosphorene anodes. *ACS Applied Materials & Interfaces*, 10(10), 8630–8639.

Mukherjee, S., Ren, Z., & Singh, G. (2018). Beyond graphene anode materials for emerging metal ion batteries and supercapacitors. *Nano-Micro Letters.,* 10(70), 1-27.

Naseri, M. (2017). Magnesium carbide monolayer: A novel quasi-planar semiconductor. *Superlattices and Microstructures*, 102, 134-140.

Naseri, M., Jalilian, J., Parandin, F., & Salehi, K. (2018). A new stable polycrystalline Be_2C monolayer: A direct semiconductor with hexa-coordinate carbons. *Physical Letters A*, 382, 2144-2148.

Nishi, Y. (2001). The development of lithium-ion secondary batteries. *Chemical Record*, 1, 406–413.

Novoselov K.S., Geim A.K., Morozov S.V., Jiang D., Zhang Y., Dubonos S.V., Grigorieva I.V., & Firsov A. A. (2004). Electric field effect in atomically thin carbon films. *Science,* 306, 666–669.

Pan, H., Hu, Y.S., & Chen, L. (2013). Room-temperature stationary sodium-ion batteries for large-scale electric energy storage. *Energy & Environmental Science*, 6, 2338-2360.

Pang, Q., Zhang, C. –L., Li, L., Fu, Z. –Q., Wei, X. –M., & Song, Y. –L. (2014). Adsorption of alkali metal atoms on germanene: A first-principles study. *Applied Surface Science*, 314, 15-20.

Park, M. H., Kim, M. G., Joo, J., Kim, K., Kim, J., Ahn, S., Cui, Y., & Cho, J. (2009). Silicon Nanotube Battery Anodes. *Nano Letters*, 9, 3844−3847.

Perdew, J. P., Burke, K., & Ernzerhof, M. (1996) Generalized gradient approximation made simple. *Physical Review Letters*, 77, 3865-3868.

Pollak, E., Geng, B., Jeon, K.-J., Lucas, I. T., Richardson, T. J., Wang, F., & Kostecki, R. (2010). The interaction of Li+ with single-layer and few-layer graphene. *Nano Letters*, 10, 3386−3388.

Ponrouch, A., Tchitchekova, D. S., Frontera, C., Barde, F., Arroyo-de Dompablo, M. E., & Palacin, M.R. (2016). Assessing Si-based anodes for Ca-ion batteries: Electrochemical decalciation of CaSi2. *Electrochemistry Communications*, 66, 75-78.

Raccichini, R., Varzi, A., Passerini, S., & Scrosati, B. (2015). The role of graphene for electrochemical energy storage. *Nature Materials,* 14, 271–279.

Rehman, J., Ali, R., Ahmad, N., Lv, X., & Guo, C. (2019). Theoretical investigation of strain- 18 engineered WSe2 monolayers as anode material for Li-ion batteries, *Journal of Alloys and Compounds*, 804, 370-375.

Scrosati, B., Hassoun, J., Sun, Y.-K. (2011) Lithium-ion batteries, A look into the future. *Energy & Environmental Science*, 4, 3287–3295.

Shi, L., & Zhao, T. (2017). Recent advances in inorganic 2D materials and their applications in lithium and sodium batteries. *Journal of Materials Chemistry A*, 5, 3735-3758.

Shi, L., Zhao, T., Xu, A., & Xu, J. (2016). Ab initio prediction of a silicene and graphene heterostructure as an anode material for Li- and Na-ion batteries. *Journal of Materials Chemistry A*, 4, 16377–16382.

Shu, H., Li, F., Hu, C., Liang, P., Cao, D., & Chen, X. (2016). The capacity fading mechanism and improvement of cycling stability in MoS2-based anode materials for lithium-ion batteries. *Nanoscale*, 8(5), 2918–2926.

Slater, M. D., Kim, D., Lee, E., & Johnson, C. S. (2012). Sodium-ion batteries. *Advanced Functional Materials*, 23(8), 947–958.

Stan, M. C., von Zamory, J., Passerini, S., Nilges, T., & Winter, M. (2013). Puzzling out the origin of the electrochemical activity of black Phosphorous as a negative electrode material for lithium-ion batteries. *Journals of Materials Chemistry A*, 1, 5293–5300.

Su, D. W., Dou, X.S., & Wang, G. X., (2015). Ultrathin MoS2 nanosheets as anode materials for sodium-ion batteries with superior performance. *Advanced Energy Materials,* 5, Article#1401205.

Sun, D., Wang, M., Li, Z., Fan, G., Fan, L. Z., & Zhou, A. (2014) Two-dimensional Ti3C2 as anode material for Li-ion batteries *Electrochemistry Communications*, 47, 80–83.

Sun, J., Zheng, G., Lee, H.-W., Liu, N., Wang, H., Yao, H., Yang, W., & Cui, Y. (2014). Formation of stable phosphorus–carbon bond for enhanced performance in black phosphorus nanoparticle–graphite composite battery anodes. *Nano Letters*, 14, 4573–4580.

Sun, Q., Dai, Y., Ma, Y., Jing, T., Wei, W, & Huang, B. (2016). Ab initio prediction and characterization of Mo_2C monolayer as anodes for lithium-ion and sodium-ion batteries. *Journal of Physical Chemistry Letters*, 7, 937-943.

Sun, Y., Zhao, L., Pan, H., Lu, X., Gu, L., Hu, Y-S., … Huang, X. (2013). Direct atomic-scale confirmation of three-phase storage mechanism in $Li_4Ti_5O_{12}$ anodes for room-temperature sodium-ion batteries. *Nature Communications*, 4, Article#1870.

Tang, Q., Zhou, Z., & Shen, P. (2012). Are MXenes promising anode materials for Li ion batteries? Computational studies on electronic properties and Li storage capability of Ti3C2 and Ti3C2X2 (X = F, OH) monolayer. *Journal of the American Chemical Society*, 134, 16909–16916.

Tian, W., Zhang, S., Huo, C., Zhu, D., Li, Q., Wang, L., Ren, X., Xie, L., Guo, S., Chu, P.K., Zeng, H., & Huo K. (2018). Few-layer antimonene: anisotropic expansion and reversible crystalline-phase evolution enable large-capacity and long-life Na-ion batteries. *ACS Nano,* 12(2), 1887-1893.

Tritsaris, G.A., Kaxiras, E., Meng, S., & Wang, E. (2013). Adsorption and diffusion of lithium on layered silicon for Li-Ion Storage. *Nano Letters*, 13, 2258-2263.

Upadhyay, S., & Srivastava, P. (2019). Modelling of antimonene as an anode material in sodium-ion battery: A first-principles study. *Materials Chemistry and Physics*, Article#122381.

Vaalma, C., Buchholz, D., Weil, M., & Passerini, S. (2018). A cost and resource analysis of sodium-ion batteries. *Nature Reviews Materials*, 3, 18013.

Vargas, C. O. A., Caballero, Á., & Morales, J. (2012). Can the performance of graphene nanosheets for lithium storage in Li-ion batteries be predicted? *Nanoscale,* 4, 2083–2092.

Vogt, P., De Padova, P., Quaresima, C., Avila, J., Frantzeskakis, E., Asensio, M. C., Resta, A., Ealet, B., & Le Lay, G. (2012). Silicene: Compelling experimental evidence for graphenelike two-dimensional silicon. *Physical Review Letters,* 108, Article#155501.

Volta, A. (1800). On the Electricity excited by the mere contact of conducting substances of different kinds. *Philosophical Transactions of the Royal Society.*, 90, 403–431.

Wang, S.S., Liu, Y. Z., Yu, Z.M., Sheng, X.L., Zhu, L., Guan, S., & Yang, S.A. (2018). Monolayer Mg_2C: Negative Poisson's ratio and unconventional two-dimensional emergent fermions. *Physical Review Materials*, 2, 104003.

Wang, Y., Song, N., Song, X., Zhang, T., Zhang, Q., & Li, M. (2018). Metallic VO_2 monolayer as an anode material for Li, Na, K, Mg or Ca ion storage: a first-principle study. *RSC Advances*, 8, 10848-10854.

Whittingham, M. S. (1974). Electrointercalation in transition-metal disulphides. *Journal of the Chemical Society, Chemical Communications*, 328–329.

Whittingham, M. S. (1976). Electrical energy storage and intercalation chemistry. *Science,* 192(4244), 1126–1127.

Wu, X., Leonard, D. P., & Ji, X. (2017). Emerging non-aqueous potassium-ion batteries: Challenges and opportunities. *Chemistry of Material,* 29, 5031–5042.

Xia, W., Zhang, Q., Xu, F., Ma, H., Chen, J., Qasim, K., Ge, B., Zhu, C., & Sun, L. (2016). Visualizing the electrochemical lithiation/delithiation behaviors of black phosphorus by in situ transmission electron microscopy. *Journal of Physical Chemistry C*, 120, 5861–5868.

Xiao, J., Choi, D., Cosimbescu, L., Koech, P., Liu, J., & Lemmon, J. P. (2010). Exfoliated MoS2 nanocomposite as an anode material for lithium-ion batteries. *Chemistry of Materials,* 22, 4522–4524.

Xie, Y., Naguib, M., Mochalin, V. N., Barsoum, M. W., Gogotsi, Y., Yu, X., … Kent, P. R. (2014). Role of surface structure on Li-ion energy storage capacity of two-dimensional transition-metal carbides. *Journal of the American Chemical Society,* 136(7), 6385–6394.

Xu, F. et al. (2016) Scalable shear-exfoliation of high-quality phosphorene nanoflakes with reliable electrochemical cycle ability in nano batteries. *2D Materials,* 3, Article#025005.

Yao, Q., Huang, C., Yuan, Y., Liu, Y., Liu, S., Deng, K., & Kan, E. (2015). Theoretical prediction of phosphorene and nanoribbons as fast-charging Li ion battery anode materials. *Journal of Physical Chemistry C,* 119(12), 6923-6928.

Yang, Z., Choi, D., Kerisit, S., Rosso, K. M., Wang, D., Zhang, J., Graff, G., & Liu, J. (2009). Nanostructures and lithium electrochemical reactivity of lithium titanites and titanium oxides: A review. *Journal of Power Sources*, 192, 588−598.

Yeoh, K.H, Chew, K-H., Chu, Y.Z., Yoon, T.L., Rusi, & Ong, D.S. (2019). First-principles study of monolayer Be2C as an anode material for lithium-ion batteries. *Journal of Applied Physics*, 126, Article#125302.

Yoshino, A., Sanechika, K., & Nakajima, T. (1985). Japanese patent no. 1989293.

Yoshio, M., Wang, H., & Fukuda, K. (2003). Spherical carbon-coated natural graphite as a lithium-ion battery-anode material. *Angewandte Chemie International Edition*, 42, 4203–4206.

Zhao, S., Kang, W., & Xue, J. (2014). The potential application of phosphorene as an anode material in Li-ion batteries. *Journal of Material Chemistry A,* 2014, 2, 19046-19052.

Zhang, J., Xu, L., Yang, C., Zhang, X., Ma, L., Zhang M., & Lu, J. (2020). Two-dimensional single-layer PC6 as promising anode materials for Li-ion batteries: The first-principles calculations study. *Applied Surface Science*, 510, Article#145493.

Zhang, S. S., & Jow, T. R. (2002). Study of Poly(acrylonitrile-methyl methacrylate) as binder for graphite anode and $LiMn_2O_4$ cathode of Li-ion batteries. *Journal of Power Sources*, 109, 422−426.

Zhang W., Liu, Y., & Guo, Z. (2019). Approaching high-performance potassium-ion batteries via advanced design strategies and engineering. *Science Advances,* 5(5), Article#7412.

Zhang, X., Jin, L., Dai, X., Chen, G., & Liu, G. (2018) Two-Dimensional GaN: an excellent electrode material providing fast ion diffusion and high storage capacity for Li-ion and Na-ion batteries. *ACS Applied Materials and Interfaces*, 10(45), 38978-38984.

Zhang, X., Meng, W., He, T., Jin L., Dai, X., & Liu, G. (2020). Mn_2C monolayer: A superior anode material offering good conductivity, high storage capacity and ultrafast ion diffusion for Li-ion and Na-ion batteries. *Applied Surface Science*, 503, Article#144091.

Zhang, X., Yang, C., Pan, Y., Weng, M., Xu, L., Liu, S., Yang, J., Yan, J. , Li, J., Shi, B., Yang, J., Zheng, J., Pan, F., & Lu, J. (2019). Monolayer GaS with high ion mobility and capacity as a promising anode battery material, *Journal of Materials Chemistry A*, 7, 14042-14050.

Zhang, X., Yu, Z., Wang, S. –S., Guan, S., Yang, H. Y., Yao, Y., & Yang. S. A. (2016). Theoretical prediction of MoN_2 monolayer as a high capacity electrode material for metal ion batteries. *Journal of Materials Chemistry A*, 4, 15224-15231.

Zhang, Z. Z., Zhang, Y.F., Li, Y., Lin, J., Truhlar, D., & Hua, S.P. (2018). MnSb2S4 monolayer as an anode material for metal-ion batteries, *Chemistry of Materials,* 30, 3208–3214.

Zhao, S., Kang, W., & Xue, J. (2014). The potential application of phosphorene as an anode material in Li-ion batteries. *Journal of Materials Chemistry A*, 2, 19046-19052.

Zheng, H., Jiang, K., Abe, T., & Ogumi, Z. (2006). Electrochemical intercalation of lithium into a natural graphite anode in quaternary ammonium-based ionic liquid electrolytes. *Carbon*, 44, 203−210.

Zhou, Y., Zhao, M., Chen, Z.W., Shi, X.M., & Jiang, Q. (2018). Potential application of 2D monolayer b-GeSe as an anode material in Na/K ion batteries. *Physical Chemistry Chemical Physics,* 20, 30290-30296

Zhu, F. F., Chen, W. J., Xu, Y., Gao, C. L., Guan, D. D., Liu, C. H., … Jia, J. F. Epitaxial growth of two-dimensional stanine. *Nature Materials*, 2015, 14(10), 1020-1025.

Zhu, J., Chroneos A., & Schwingenschlogl, U. (2016). Silicene/germanene on MgX2 (X = Cl, Br, and I) for Li-ion battery applications. *Nanoscale*, 8, 7272–7277.

Zhu, J., & Schwingenschlögl, U. (2017). P and Si functionalized MXenes for metal-ion battery applications. *2D Materials*, 4, Article#025073.